applied sciences

MDPI

Article

Continuous Rotor Dynamics of Multi-Disc and Multi-Span Rotor: A Theoretical and Numerical Investigation on the Continuous Model and Analytical Solution for Unbalance Responses

Aiming Wang [1,*], Yujie Bi [2], Yun Xia [1], Xiaohan Cheng [1], Jie Yang [1] and Guoying Meng [1]

[1] School of Mechanical Electronic & Information Engineering, China University of Mining & Technology (Beijing), Beijing 100083, China; xiayun@cumtb.edu.cn (Y.X.); chengxh@cumtb.edu.cn (X.C.); 201702@cumtb.edu.cn (J.Y.); mgy@cumtb.edu.cn (G.M.)

[2] School of Mechanics and Civil Engineering, China University of Mining & Technology (Beijing), Beijing 100083, China; byjpengqiao@126.com

* Correspondence: wam_master@163.com; Tel.: +86-134-8871-3431

Abstract: Continuous rotor dynamics remains stagnant. In this paper, aim at multi-span and multi-disc rotor-bearing system, the continuous rotor dynamic analysis method (CRDAM) is proposed. The force acting on the shaft by the rotating eccentric disc is simulated as a point force. The counterforce of bearing is also considered as a point force. The shaft is considered free-ended. A continuous rotor dynamic model is obtained and an analytical solution is proposed to express the unbalance response as function of the position, unbalance, support stiffness and damping. The proposed method is validated by numerical experiments in which unbalance responses obtained by it are compared with that obtained by the two classical methods the finite element method (FEM) and Ricatti method. The results indicate that the proposed method is applicable to calculating unbalance response of multi-disc and multi-span rotor. Moreover, it is closer to FEM than Ricatti and can be applied to actual high speed rotors. Among the three methods, the calculating speed of Ricatti is the fastest, CRDAM is the second fastest and FEM is the slowest. The proposed method, which solves the forward problems of the continuous rotor dynamics for the multi-disc and multi-span rotors, can provide theoretical basis for further studies on inverse problems such as identification of rotor unbalance and bearing stiffness and damping coefficients without test runs and external excitations.

Keywords: continuous rotor dynamics; multi-span and multi-disc rotor-bearing system; continuous rotor dynamic analysis method; continuous rotor dynamic model; analytical solution

check for updates

Citation: Wang, A.; Bi, Y.; Xia, Y.; Cheng, X.; Yang, J.; Meng, G. Continuous Rotor Dynamics of Multi-Disc and Multi-Span Rotor: A Theoretical and Numerical Investigation on the Continuous Model and Analytical Solution for Unbalance Responses. *Appl. Sci.* **2022**, *12*, 4351. https://doi.org/10.3390/app12094351

Academic Editor: Jan Awrejcewicz

Received: 17 March 2022
Accepted: 22 April 2022
Published: 25 April 2022

1. Introduction

Rotor Dynamics, which has been concerned all the time, is an old research field. It is the mechanical basis for the design, manufacture, safe operation and fault diagnosis of rotating machinery. There are forward and inverse problems of rotor dynamics. The forward problem is to study dynamic responses of rotors with known rotor parameters and loads, while for the inverse problem, it is identification of rotor parameters and loads from dynamic responses. This paper is focused on the forward problem which is continuous model and analytical solution of unbalance response of multi-disc and multi-span rotor. The continuous rotor dynamic analysis method proposed can be applied to studying the inverse problems which are rotor unbalance identification algorithm and bearing coefficients identification algorithm, respectively.

In order to determine the unbalance response of the system, the Ricatti method [1–6] and the Finite Elements method (FEM) [6–13] are proposed, which are based on discrete model. Although these methods can be used to predict the unbalance vibration for a complicated rotor system, it remains hard to be applied to the identification of bearing dynamic parameters, estimation of rotor unbalance and balancing of rotor systems. It is because their model are discrete and the unbalance response can not be expressed as a function of position, rotor unbalance and stiffness and damping coefficients of bearings. Hence, it's difficult to identify rotor unbalance and bearing dynamic parameters by solving the equations which are built using the unbalance responses at some positions on rotor-shaft as known conditions.

For the continuous beam model of rotor systems, in the literature there exist limited numbers of studies that concentrate on the analytical modeling of rotor systems. Euler-Bernoulli beam [14], Rayleigh beam [14–18] and Timoshenko beam [19] are three kinds of continuous beam models for unbalanced rotor-bearing system. Based on Euler-Bernoulli model, vibration analysis of beams with multiple steps and different shapes of cross section were conducted [20]. Heydari [21] carried out free vibration analysis of the Euler-Bernoulli shaft with two rigid bearings and a flexible disk to study the influence of the disk's location and aspect ratio on natural frequencies and critical speeds. Varanis [22] presented a continuous rotor model for rubbing applications based on Euler-Bernoulli continuous model considering transverse shear, rotatory inertia, and gyroscopic moments and Wavelet Techniques was used to study the response for detection and characterization of rubbing phenomenon. Zhou provided a method to obtain the analytical imbalance response of the Jeffcott rotor under constant acceleration [23]. Lee [24] studied an axially-loaded Euler-Bernoulli shaft, clamped at one end with an intermediate spring support. That work placed the equations of motion into state-space form to find critical speeds. The same approach was applied to shafts with rectangular cross-sections for examining the stability of pretwisted simply-supported rotating beams [25] and various end conditions that are different in orthogonal directions relative to the rotating shaft [26]. Chun and Lee [27] modeled an Euler-Bernoulli shaft with a single bladed disk using the Ritz method for both shaft and blades. Lee and Chun [28] incorporated flexible disks into the Ritz series analysis for modeling hard disk drives. More specific applications using this method were performed by Hamidi et al. [29] for a rotating, cracked Euler-Bernoulli shaft. Wang [30] proposed an analytical solution of unbalance responses for single-span and single-disc rotor-bearing systems and an identification method for rotor unbalance was given. To investigate rotor dynamics, such as the vibration problem, the influence of the number of blade and rotating speed on the natural frequencies, Euler-Bernoulli theory were employed along with FEM [31,32]. According to Rayleigh model, unbalance responses are expressed as a function of position on the rotor-shaft, rotor unbalance and bearing coefficients [33]. Using the Rayleigh beam model and Timoshenko model, mathematical modeling of continuous multi-stepped rotor-bearing systems was presented and the partial differential equations were discretized to obtain a close-form solution [34,35]. According to Timoshenko theory, Farghaly, Afshari and Torabi presented methods for multi-stepped beams with attachments [36], multi-stepped rotors [37] and multi-span multi-stepped shafts resting on multiple bearings [38] and rotors with multiple concentrated masses [39]. Using Timoshenko beam theory combined with FEM, Rao [40] studied dynamic responses of bidirectional functionally graded rotor shaft. It is found that the obtained dynamic responses are influenced by temperature variation, power-law index and internal viscous and hysteretic damping. Felice [41] modelled the rotor-shaft as a spinning Timoshenko beam and derived analytical expressions for critical solutions to analyze damping gyroscopic effects on the stability of parametrically excited continuous rotor systems. Hsu [42] obtained equations of motion for a Timoshenko shaft with flexible disks which were solved numerically to obtain the time domain response. Although Wang [30,33] proposed an analytical solution of a continuous rotor-baring system supported with two bearings and a disc, the solution cannot be applied to rotors with multi bearing and muti disc. Moreover, with regard to forces of the bearings and disc, the continuous model of a rotor-bearing system is a fourth-order non homogeneous partial differential equation set with homogeneous boundary condition. There is no universal method to solve them so far. When using integral transform method to solve the equation, it is difficult to achieve the inverse transformation. While for the separation of variables method, it can only be used to solve the homogeneous partial differential equation set with homogeneous boundary condition.

In this paper, the continuous rotor dynamic analysis method (CRDAM) is proposed for multi-disc and multi-span rotor represented by the homogeneous and elastic Rayleigh beam. Forces of the bearings and discs are considered as point forces. free-ended boundary condition is used in modelling the rotor. A continuous model, which is a fourth-order non-homogeneous partial differential equation set with homogeneous boundary condition, is developed. An analytical solution is proposed to express the unbalance response as a function of position, rotor unbalance and the stiffness and damping coefficients of bearings. Numerical simulations are conducted to validate the proposed method. The accuracy of the proposed method is higher than the Ricatti method and the calculating speed is faster than FEM. It can be applied to the identification of rotor unbalance and bearing coefficients for multi-disc and multi-span rotors.

The remainder of this paper is organized as follows. Section 2 describes the continuous model of the multi-disc and multi-span rotors and its analytical solution. Section 3 is the validation of the proposed method by numerical simulations of rotors supported with rolling bearings and oil-journal bearings. Section 4 describes the main conclusions.

2. Theory

2.1. Continous Model Based on Rayleigh Model

The multi-disc and multi-span rotor-bearing system, which has m discs and n bearings, is shown in Figure 1. The force analysis of micro-element is shown in Figure 2. Regarding the connection between shafts as a rigid connection and using Rayleigh's theory [14–16,33,43] in which the shaft is regarded a perfect elastic body (It is homogeneous and isotropic and obeys Hooke's Law) and the moment of inertia of rotor-shaft is considered, the relationship between the lateral displacement of rotor-shaft in x and y directions and the excitation can be described as following according to Figure 2.

$$EI\frac{\partial^4 y}{\partial z^4} + m\frac{\partial^2 y}{\partial t^2} - \left(I_{dx}\frac{\partial^4 y}{\partial z^2 \partial t^2} + I_p w\frac{\partial^3 x}{\partial z^2 \partial t} \right) = f_y \quad (1)$$

$$EI\frac{\partial^4 x}{\partial z^4} + m\frac{\partial^2 x}{\partial t^2} - \left(I_{dy}\frac{\partial^4 x}{\partial z^2 \partial t^2} - I_p w\frac{\partial^3 y}{\partial z^2 \partial t} \right) = f_x \quad (2)$$

where x and y are the lateral displacement components due to lateral vibrations of the rotor shaft in the natural coordinates; z is the axial position of the shaft; t is the time; m is the mass per unit length of rotor-shaft; w is the rotation frequency; I_p is the polar moment of inertia per unit length of the shaft; I_{dx} is the diameter moments of inertia per unit length of the shaft in the x directions. $\theta_x(z,t)$ and $\theta_y(z,t)$ is the rotation angle of the micro-element around x-axis and y-axis, respectively; T_y is the shear force on the left end of the micro-element in y direction; M_x is the moment on the left end of the micro-element in yoz plane; f_y is the external force in y direction on the micro-element of the shaft; I_{dy} is the diameter moments of inertia per unit length of the shaft in the y directions; T_x is the shear force on the left end of the micro-element in x direction; M_y is the moment on the left end of the micro-element in xoz plane; f_x is the external force in x direction on the micro-element of the shaft; E is the elastic modulus of the shaft; I is the diametric shaft cross-sectional geometric moment of inertia.

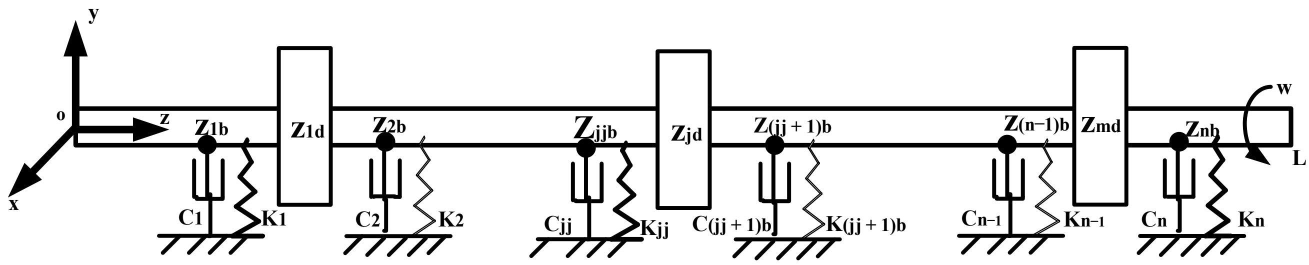

Figure 1. Multi-disc and multi-span rotor-bearing system.

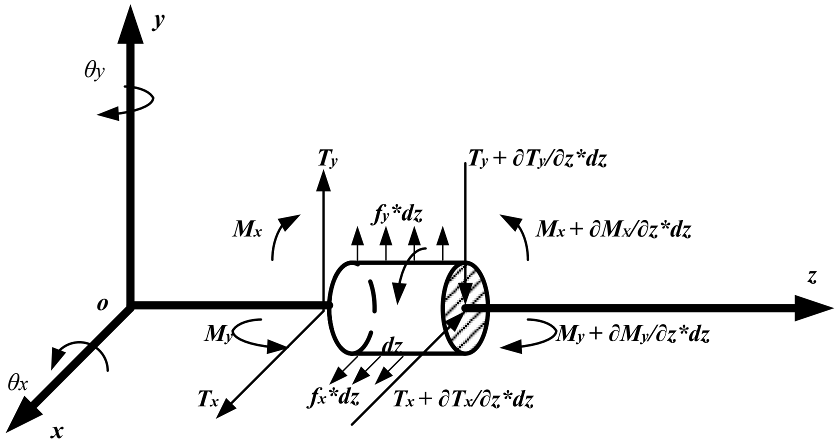

Figure 2. Physical model of the system.

The force of each bearing acting on the shaft can be expressed as following.

$$f_{ib\cdot y} = \left(k_{i\cdot yx}x_{ib} + k_{i\cdot yy}y_{ib} + c_{i\cdot yx}\frac{\partial x_{ib}}{\partial t} + c_{i\cdot yy}\frac{\partial y_{ib}}{\partial t}\right)\delta(z - z_{ib}) \quad (3)$$

$$f_{ib\cdot x} = \left(k_{i\cdot xx}x_{ib} + k_{i\cdot xy}y_{ib} + c_{i\cdot xx}\frac{\partial x_{ib}}{\partial t} + c_{i\cdot xy}\frac{\partial y_{ib}}{\partial t}\right)\delta(z - z_{ib}) \quad (4)$$

where i is from 1 to n; $k_{i\cdot xx}$, $k_{i\cdot xy}$, $k_{i\cdot yy}$ and $k_{i\cdot yx}$ are the four stiffness coefficients of #i bearing; $c_{i\cdot xx}$, $c_{i\cdot xy}$, $c_{i\cdot yy}$ and $c_{i\cdot yx}$ are the four damping coefficients of #i bearing; z_{ib} is the z coordinate position of #i bearing; y_{ib} and x_{ib} are the lateral displacement components due to lateral vibrations of the rotor shaft in position z_{ib}.

The force of the eccentric disc acting on the shaft can be expressed as following.

$$f_{jd\cdot y} = \left(m_{ju}w^2e_j\sin(wt + \alpha_j) - m_{j\cdot d}\frac{\partial^2 y_{jd}}{\partial t^2}\right)\delta\left(z - z_{jd}\right) \quad (5)$$

$$f_{jd\cdot x} = \left(m_{ju}w^2e_j\cos(wt + \alpha_j) - m_{j\cdot d}\frac{\partial^2 x_{jd}}{\partial t^2}\right)\delta\left(z - z_{jd}\right) \quad (6)$$

where j is from 1 to m; m_{jd} is the mass of #j disc; m_{ju} is the eccentric mass of #j disc; e_j is the eccentric distance of #j disc; α_j is the eccentric angle of #j disc; z_{jd} is the z coordinate position of #j disc.

Hence, the external force acting on the shaft by the disc and bearing is

$$f_y = \sum_{i=1}^{n} f_{ib\cdot y} + \sum_{j=1}^{m} f_{jd\cdot y} \quad (7)$$

$$f_x = \sum_{i=1}^{n} f_{ib\cdot x} + \sum_{j=1}^{m} f_{jd\cdot x} \tag{8}$$

Free-ended boundary condition can be used in the modeling. The flexural torque and shearing force at both ends are zero. Hence, Equations (9) and (10) can be obtained.

$$\begin{cases} EI\frac{\partial^2}{\partial z^2}y(z,t)|_{z=0,L} = 0 \\ EI\frac{\partial^3}{\partial z^3}y(z,t)|_{z=0,L} = 0 \end{cases} \tag{9}$$

$$\begin{cases} EI\frac{\partial^2}{\partial z^2}x(z,t)|_{z=0,L} = 0 \\ EI\frac{\partial^3}{\partial z^3}x(z,t)|_{z=0,L} = 0 \end{cases} \tag{10}$$

where L is the total length of rotor-shaft.

To obtain dimensionless model, the following dimensionless quantities in Table 1 are defined.

Table 1. Dimensionless quantities for the dimensionless model of the continuous rotor.

Symbols	Description
$u = y/L$	u is the dimensionless lateral displacement of the shaft in y direction.
$v = x/L$	v is the dimensionless lateral displacement of the shaft in x direction.
$q = z/L$	q is the dimensionless quantityy of z.
$q_{ib} = z_{ib}/L$	q_{ib} is the dimensionless z_{ib}; z_{ib} is the position of NO. i bearing; $i = 1 - n$.
$u_{ib} = y_{ib}/L$	u_{ib} is the dimensionless lateral displacement of the shaft in y direction at position z_{ib}.
$v_{ib} = x_{ib}/L$	v_{ib} is the dimensionless lateral displacement of the shaft in x direction at position z_{ib}.
$q_{jd} = z_{jd}/L$	q_{jd} is the dimensionless z_{jd}; z_{jd} is the position of the number j disc; $j = 1 - m$.
$u_{jd} = y_{jd}/L$	u_{jd} is the dimensionless lateral displacement of the shaft in y direction at position z_{jd}.
$v_{jd} = x_{jd}/L$	v_{jd} is the dimensionless lateral displacement of the shaft in x direction at position z_{jd}.

Therefore, the dimensionless partial differential equations of the lateral vibration of a rotating shaft motion in the unbalanced multi-disc and multi-span rotor-bearing system can be expressed in the form of Equations (11) and (12) according to Equations (1) and (2) and Equations (7) and (8).

$$\begin{aligned} &\frac{\partial^4 u}{\partial q^4} + \frac{mL^4}{EI}\frac{\partial^2 u}{\partial t^2} - \left(\frac{I_{dx}L^2}{EI}\frac{\partial^4 u}{\partial q^2 \partial t^2} + \frac{I_p L^2 w}{EI}\frac{\partial^3 v}{\partial q^2 \partial t}\right) = \frac{L^3}{EI}\Bigg\{ \\ &\sum_{j=1}^{m}\left[\left(\pi m_{ju} w^2 e_j \sin(wt+\alpha_j) - m_{jd} L \frac{\partial^2 u_{jd}}{\partial t^2}\right)\delta\Big(L\big(q-q_{jd}\big)\Big)\right] \\ &-\sum_{i=1}^{n}\left[\left(k_{i\cdot yx} L v_{ib} + k_{i\cdot yy} L u_{ib} + c_{i\cdot yx} L \frac{\partial v_{ib}}{\partial t} + c_{i\cdot yy} L \frac{\partial u_{ib}}{\partial t}\right)\delta(L(q-q_{ib}))\right] \quad \Bigg\} \end{aligned} \tag{11}$$

$$\begin{aligned} &\frac{\partial^4 v}{\partial q^4} + \frac{mL^4}{EI}\frac{\partial^2 v}{\partial t^2} - \left(\frac{I_{dy}L^2}{EI}\frac{\partial^4 v}{\partial q^2 \partial t^2} - \frac{I_p L^2 w}{EI}\frac{\partial^3 u}{\partial q^2 \partial t}\right) = \frac{L^3}{EI}\Bigg\{ \\ &\sum_{j=1}^{m}\left[\left(\pi m_{ju} w^2 e_j \cos(wt+\alpha_j) - m_{jd} L \frac{\partial^2 v_{jd}}{\partial t^2}\right)\delta\Big(L\big(q-q_{jd}\big)\Big)\right] \\ &-\sum_{i=1}^{n}\left[\left(k_{i\cdot xx} L v_{ib} + k_{i\cdot xy} L u_{ib} + c_{i\cdot xx} L \frac{\partial u_{ib}}{\partial t} + c_{i\cdot xy} L \frac{\partial v_{ib}}{\partial t}\right)\delta(L(q-q_{ib}))\right] \quad \Bigg\} \end{aligned} \tag{12}$$

where m_{jd} is the mass of #j disc; m_{ju} is the eccentric mass of #j disc; α_j which is defined as the angle contained by the x-axis and the eccentric position in the direction of rotation is the eccentric angle of #j disc; e_j is #j disc's eccentric distance; $\delta()$ is the Dirac's function; $k_{i\cdot xx}$, $k_{i\cdot xy}$, $k_{i\cdot yy}$, $k_{i\cdot yx}$ are the stiffness coefficients of #i bearing; $c_{i\cdot xx}$, $c_{i\cdot xy}$, $c_{i\cdot yy}$, $c_{i\cdot yx}$ are the damping coefficients of #i bearing.

The dimensionless form of the free-ended boundary condition in Equations (9) and (10) are:

$$\begin{cases} \frac{\partial^2}{\partial q^2} u(q,t)|_{q=0,1} = 0 \\ \frac{\partial^3}{\partial q^3} u(q,t)|_{q=0,1} = 0 \end{cases} \tag{13}$$

$$\begin{cases} \frac{\partial^2}{\partial q^2} v(q,t)|_{q=0,1} = 0 \\ \frac{\partial^3}{\partial q^3} v(q,t)|_{q=0,1} = 0 \end{cases} \tag{14}$$

2.2. Analytical Solution

According to the fourier transform of Equations (11) and (12) on the variable t and considering that the frequency of the unbalance response is equal to the rotation frequency w, the dimensionless unbalance responses in frequency domain satisfy Equations (15) and (16).

$$\begin{aligned}
&\frac{\partial^4 U}{\partial q^4} - \frac{m \cdot w^2 L^4}{EI} U + \frac{I_{dx} L^2 w^2}{EI} \frac{\partial^2 U}{\partial q^2} - \frac{i \cdot w^2 I_p L^2}{EI} \frac{\partial^2 V}{\partial q^2} \\
&= \{ [m_{1u} w^2 e_1 \pi (\sin\alpha_1 - i \cdot \cos\alpha_1) + w^2 m_{1d} L U_{1d}] \delta(q - q_{1d}) \\
&+ \cdots\cdots \\
&+ [m_{mu} w^2 e_m \pi (\sin\alpha_m - i \cdot \cos\alpha_m) + w^2 m_{md} L U_{md}] \delta(q - q_{md}) \\
&- L\Big(k_{1b \cdot yx} V_{1b} + k_{1b \cdot yy} U_{1b} + i \cdot w c_{1b \cdot yx} V_{1b} + i \cdot w c_{1b \cdot yy} U_{1b}\Big) \delta(q - q_{1b}) \\
&- L\Big(k_{2b \cdot yx} V_{2b} + k_{2b \cdot yy} U_{2b} + i \cdot w c_{2b \cdot yx} V_{2b} + i \cdot w c_{2b \cdot yy} U_{2b}\Big) \delta(q - q_{2b}) \\
&+ \cdots\cdots \\
&- L\Big(k_{nb \cdot yx} V_{nb} + k_{nb \cdot yy} U_{nb} + i \cdot w c_{nb \cdot yx} V_{nb} + i \cdot w c_{nb \cdot yy} U_{nb}\Big) \delta(q - q_{nb}) \Big\} \frac{L^2}{EI}
\end{aligned} \tag{15}$$

$$\begin{aligned}
&\frac{\partial^4 V}{\partial q^4} - \frac{w^2 m L^4}{EI} V + \frac{w^2 I_{dx} L^2}{EI} \frac{\partial^2 V}{\partial q^2} + \frac{i \cdot w^2 I_p L^2}{EI} \frac{\partial^2 U}{\partial q^2} \\
&= \{ [m_{1u} w^2 e_1 \pi (\cos\alpha_1 + i \cdot \sin\alpha_1) + w^2 m_{1d} L V_{1d}] \delta(q - q_{1d}) \\
&+ \cdots\cdots \\
&+ [m_{mu} w^2 e_m \pi (\cos\alpha_m + i \cdot \sin\alpha_m) + w^2 m_{md} L V_{md}] \delta(q - q_{md}) \\
&- L\Big(k_{1b \cdot xx} V_{1b} + k_{1b \cdot xy} U_{1b} + i \cdot w c_{1b \cdot xx} V_{1b} + i \cdot w c_{1b \cdot xy} U_{1b}\Big) \delta(q - q_{1b}) \\
&- L\Big(k_{2b \cdot xx} V_{2b} + k_{2b \cdot xy} U_{2b} + i \cdot w c_{2b \cdot xx} V_{2b} + i \cdot w c_{2b \cdot xy} U_{2b}\Big) \delta(q - q_{2b}) \\
&- \cdots\cdots \\
&- L\Big(k_{nb \cdot xx} V_{nb} + k_{nb \cdot xy} U_{nb} + i \cdot w c_{nb \cdot xx} V_{nb} + i \cdot w c_{nb \cdot xy} U_{nb}\Big) \delta(q - q_{nb}) \Big\} \frac{L^2}{EI}
\end{aligned} \tag{16}$$

where U and V are the dimensionless unbalance responses in frequency domain in x and y directions.

$U(q)$ and $V(q)$ can be expressed using Green Function as following.

$$U(q) = \frac{L^2}{EI} \begin{bmatrix} \pi m_{1u} w^2 e_1 (\sin\alpha_1 - i \cdot \cos\alpha_1) + w^2 m_{1d} L U_{1d} \\ \vdots \\ \pi m_{mu} w^2 e_m (\sin\alpha_m - i \cdot \cos\alpha_m) + w^2 m_{md} L U_{md} \\ -L(k_{1 \cdot yx} V_{1b} + k_{1 \cdot yy} U_{1b} + i \cdot w c_{1 \cdot yx} V_{1b} + i \cdot w c_{1 \cdot yy} U_{1b}) \\ \vdots \\ -L(k_{n \cdot yx} V_{nb} + k_{n \cdot yy} U_{nb} + i \cdot w c_{n \cdot yx} V_{nb} + i \cdot w c_{n \cdot yy} U_{nb}) \end{bmatrix}_{(m+n)\times 1}^{T} \begin{bmatrix} G_u(q, q_{1d}) \\ \vdots \\ G_u(q, q_{md}) \\ G_u(q, q_{1b}) \\ \vdots \\ G_u(q, q_{nb}) \end{bmatrix}_{(m+n)\times 1} \tag{17}$$

$$V(q) = \frac{L^2}{EI} \begin{bmatrix} \pi m_{u1} w^2 e_1 (\cos\alpha_1 + i \cdot \sin\alpha_1) + w^2 m_{1d} L V_{1d} \\ \vdots \\ \pi m_{mu} w^2 e_m (\cos\alpha_m + i \cdot \sin\alpha_m) + w^2 m_{md} L V_{md} \\ -L(k_{1 \cdot xx} V_{1b} + k_{1 \cdot xy} U_{1b} + i \cdot w c_{1 \cdot xx} V_{1b} + i \cdot w c_{1 \cdot xy} U_{1b}) \\ \vdots \\ -L(k_{n \cdot xx} V_{nb} + k_{n \cdot xy} U_{nb} + i \cdot w c_{n \cdot xx} V_{nb} + i \cdot w c_{n \cdot xy} U_{nb}) \end{bmatrix}_{(m+n)\times 1}^{T} \begin{bmatrix} G_v(q, q_{1d}) \\ \vdots \\ G_v(q, q_{md}) \\ G_v(q, q_{1b}) \\ \vdots \\ G_v(q, q_{nb}) \end{bmatrix}_{(m+n)\times 1} \tag{18}$$

where $G_u(q, q_{1d})$, $G_u(q, q_{md})$, $G_u(q, q_{1b})$, $G_u(q, q_{2b})$, $G_u(q, q_{nb})$, $G_v(q, q_{1d})$, $G_v(q, q_{md})$, $G_v(q, q_{1b})$, $G_v(q, q_{2b})$ and $G_v(q, q_{nb})$ are Green's coefficients. Further, U_{1d}, U_{md}, U_{1b}, U_{2b}, U_{nb}, V_{1d}, V_{md},

V_{1b}, V_{2b} and V_{nb} represent the dimensionless unbalance response of the bearings and discs in the frequency domain.

The above-mentioned Green's coefficients can be calculated using Equation (19) which is derived in reference [33].

$$\begin{bmatrix} G_u(q,q_i) \\ G_v(q,q_i) \end{bmatrix} = \begin{bmatrix} \sum_{j=1}^{8} \frac{f_1(s_j)e^{s_j \cdot q}}{f'(s_j)} & \sum_{j=1}^{8} \frac{f_2(s_j)e^{s_j \cdot q}}{f'(s_j)} & \sum_{j=1}^{8} \frac{i \cdot KPs_j e^{s_j \cdot q}}{f'(s_j)} & \sum_{j=1}^{8} \frac{i \cdot KPe^{s_j \cdot q}}{f'(s_j)} & \sum_{j=1}^{8} \frac{f_3(s_j)e^{s_j \cdot q}}{f'(s_j)e^{-q_i s_j}} \\ \sum_{j=1}^{8} \frac{-i \cdot KPs_j e^{s_j \cdot q}}{f'(s_j)} & \sum_{j=1}^{8} \frac{-i \cdot KPe^{s_j \cdot q}}{f'(s_j)} & \sum_{j=1}^{8} \frac{f_1(s_j)e^{s_j \cdot q}}{f'(s_j)} & \sum_{j=1}^{8} \frac{f_2(s_j)e^{s_j \cdot q}}{f'(s_j)} & \sum_{j=1}^{8} \frac{f_4(s_j)e^{s_j \cdot q}}{f'(s_j)e^{-q_i s_j}} \end{bmatrix} \begin{bmatrix} A_i \\ B_i \\ C_i \\ D_i \\ u(q-q_i) \end{bmatrix} \tag{19}$$

where $K = \frac{w^2 mL^4}{EI}$; $P = \frac{I_p w^2 L^2}{EI}$; $u(q-q_i)$ is the Heaviside function; $s_j(j = 1–8)$ are the solutions of $f(s) = 0$; $f(s)$, $f_1(s)$, $f_2(s)$, $f_3(s)$, $f_4(s)$ and $f'(s)$ can be obtained using Equation (20); $L_1 = \frac{I_{dx} w^2 L^2}{EI} = \frac{I_{dy} w^2 L^2}{EI}$; $\begin{bmatrix} A_i \\ B_i \\ C_i \\ D_i \end{bmatrix} = -[M_{11}]^{-1} \cdot [M_{12}]$, the two matrices M_{11} and M_{12} can be found in Equations (A1) and (A2) in Appendix A.

$$\begin{bmatrix} f(s) \\ f_1(s) \\ f_2(s) \\ f_3(s) \\ f_4(s) \\ f'(s) \end{bmatrix} = \begin{bmatrix} s^8 + 2L_1 s^6 + \left(-2K + L_1{}^2 - P^2\right)s^4 - 2L_1 K s^2 + K^2 \\ s^7 + 2L_1 s^5 + \left(L_1{}^2 - P^2 - K\right)s^3 - KL_1 s \\ s^6 + 2L_1 S^4 + \left(L_1{}^2 - P^2 - K\right)s^2 - KL_1 \\ s^4 + (L_1 + i \cdot P)s^2 - K \\ s^4 + (L_1 - i \cdot P)s^2 - K \\ 8s^7 + 12s^5 + 4\left(L_1{}^2 - P^2 - 2K\right)s^3 - 4L_1 Ks \end{bmatrix} \tag{20}$$

$m + n$ equations can be obtained by substituting $q = q_{1d},\ldots, q = q_{md},\ldots, q = q_{1b}, q = q_{mb}$ in Equations (17) and (18), respectively. The obtained equation can be expressed in a matrix form as follows:

$$H_1 = H_2 \cdot H_3 \tag{21}$$

where $H_3 = \begin{bmatrix} U_{1d} \cdots U_{md} & V_{1d} \cdots V_{md} & U_{1b} \cdots U_{nb} & V_{1b} \cdots V_{nb} \end{bmatrix}$

$$H_1 = \begin{bmatrix} -\pi m_{1u} w^2 e_1 (\sin\alpha_1 - i \cdot \cos\alpha_1) G_u(q_{1d}, q_{1d}) - \cdots\cdots - \pi m_{mu} w^2 e_m (\sin\alpha_m - i \cdot \cos\alpha_m) G_u(q_{1d}, q_{md}) \\ \vdots \\ -\pi m_{1u} w^2 e_1 (\sin\alpha_1 - i \cdot \cos\alpha_1) G_u(q_{md}, q_{1d}) - \cdots\cdots - \pi m_{mu} w^2 e_m (\sin\alpha_m - i \cdot \cos\alpha_m) G_u(q_{md}, q_{md}) \\ -\pi m_{1u} w^2 e_1 (\cos\alpha_1 + i \cdot \sin\alpha_1) G_v(q_{1d}, q_{1d}) - \cdots\cdots - \pi m_{mu} w^2 e_m (\cos\alpha_m + i \cdot \sin\alpha_m) G_v(q_{1d}, q_{md}) \\ \vdots \\ -\pi m_{1u} w^2 e_1 (\cos\alpha_1 + i \cdot \sin\alpha_1) G_v(q_{md}, q_{1d}) - \cdots\cdots - \pi m_{mu} w^2 e_m (\cos\alpha_m + i \cdot \sin\alpha_m) G_v(q_{md}, q_{md}) \\ -\pi m_{1u} w^2 e_1 (\sin\alpha_1 - i \cdot \cos\alpha_1) G_u(q_{1b}, q_{1d}) - \cdots\cdots - \pi m_{mu} w^2 e_m (\sin\alpha_m - i \cdot \cos\alpha_m) G_u(q_{1b}, q_{md}) \\ -\pi m_{1u} w^2 e_1 (\sin\alpha_1 - i \cdot \cos\alpha_1) G_u(q_{2b}, q_{1d}) - \cdots\cdots - \pi m_{mu}{}^2 e_m (\sin\alpha_m - i \cdot \cos\alpha_m) G_u(q_{2b}, q_{md}) \\ \vdots \\ -\pi m_{1u} w^2 e_1 (\sin\alpha_1 - i \cdot \cos\alpha_1) G_u(q_{nb}, q_{1d}) - \cdots\cdots - \pi m_{mu} w^2 e_m (\sin\alpha_m - i \cdot \cos\alpha_m) G_u(q_{nb}, q_{md}) \\ -\pi m_{1u} w^2 e_1 (\cos\alpha_1 + i \cdot \sin\alpha_1) G_v(q_{1b}, q_{1d}) - \cdots\cdots - \pi m_{mu} w^2 e_m (\cos\alpha_m + i \cdot \sin\alpha_m) G_v(q_{1b}, q_{md}) \\ -\pi m_{1u} w^2 e_1 (\cos\alpha_1 + i \cdot \sin\alpha_1) G_v(q_{2b}, q_{1d}) - \cdots\cdots - \pi m_{mu} w^2 e_m (\cos\alpha_m + i \cdot \sin\alpha_m) G_v(q_{2b}, q_{md}) \\ \vdots \\ -\pi m_{1u} w^2 e_1 (\cos\alpha_1 + i \cdot \sin\alpha_1) G_v(q_{nb}, q_{1d}) - \cdots\cdots - \pi m_{mu} w^2 e_m (\cos\alpha_m + i \cdot \sin\alpha_m) G_v(q_{nb}, q_{md}) \end{bmatrix}$$

$$H_2 = \begin{bmatrix} H_{11} & H_{12} & H_{13} & H_{14} \\ H_{21} & H_{22} & H_{23} & H_{24} \\ H_{31} & H_{32} & H_{33} & H_{34} \\ H_{41} & H_{42} & H_{43} & H_{44} \end{bmatrix}_{2(m+n)\times 2(m+n)} - \begin{bmatrix} \frac{L^2}{EI} & & & \\ & \ddots & & \\ & & \ddots & \\ & & & \frac{L^2}{EI} \end{bmatrix}_{2(m+n)\times 2(m+n)}$$

The sub-matrixes of H_2 are in Equations (A3)–(A18) in Appendix A.

According to Equation (21), $U_{1d}\ldots U_{md}$, $V_{1d}\ldots V_{md}$, $U_{1b}\ldots U_{nb}$, $V_{1b}\ldots V_{nb}$ can be expressed as follows:

$$\begin{bmatrix} U_{1d}\cdots U_{md} & V_{1d}\cdots V_{md} & U_{1b}\cdots U_{nb} & V_{1b}\cdots V_{nb} \end{bmatrix} = {H_2}^{-1}\cdot H_1 \tag{22}$$

Hence, as shown in Figure 3, the dimensionless unbalance response in frequency domain can be calculated using Equations (17) and (18) in which the unknown Green's coefficients can be calculated based on Equation (19) and the dimensionless unbalance response of the bearings and discs can be calculated using Equation (22).

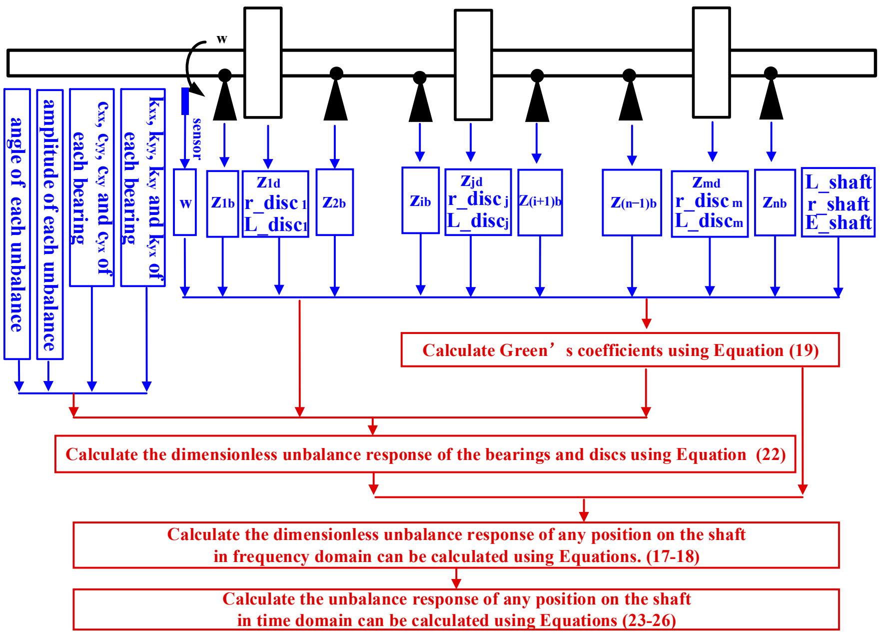

Figure 3. Flowchart of the proposed CRDAM.

Thus, the unbalance response in frequency domain can be expressed as following.

$$Y(z) = U(q)L \tag{23}$$

$$X(z) = V(q)L \tag{24}$$

Change $Y(z)$ and $X(z)$ from frequency domain to time domain and the following are obtained:

$$y(z,t) = \frac{\mathrm{abs}(Y(z))}{\pi}\cos(wt + \mathrm{angle}(Y(z))) \tag{25}$$

$$x(z,t) = \frac{\mathrm{abs}(X(z))}{\pi}\cos(wt + \mathrm{angle}(X(z))) \tag{26}$$

where abs() is the amplitude of a complex number; angle() is the angle of a complex number.

3. Numerical Simulations and Discussion

3.1. Methodology of Numerical Simulations

The aim of the numerical simulation is to validate the proposed CRDAM. The Ricatti and FEM results are taken as the references. The Ricatti method, which has the advantage of fast calculation speed and low requirement for CPU, is an old classical method to obtain rotor dynamic characteristics. With the rapid development of computes, the FEM method becomes an effective and commonly used method for calculating rotor dynamic characteristics of rotors, especially for large rotors. In the simulations, critical frequencies and unbalance responses of the three methods are obtained to conduct the comparison among them for the validation. When relative errors and absolute errors are used to quantitatively analyze the difference of calculated critical frequencies and unbalance responses among three method, FEM results are treated as the base-exact.

18 computational examples are used in the simulation. Figures 4–12 shows nine kinds of rotors. They represent five-span and five-disc rotor, single-span and five-disc rotor, four-span and four-disc rotor, three-span and three-disc rotor, two-span and two-disc rotor, single-span and single-disc rotor, single-span and four-disc rotor, single-span and three-disc rotor and single-span and two-disc rotor. The 18 computational examples are the nine kinds rotors with oil-journal bearings and nine kinds rotors with rolling bearings. g1.1, g1.2, g1.3, g1.4, g1.5, g2.2, g3.3, g4.4 and g5.5 are the nine kinds of rotors with rolling bearings and h1.1, h1.2, h1.3, h1.4, h1.5, h2.2, h3.3, h4.4 and h5.5 the nine kinds rotors with oil-journal bearings. The parameters of the bearings, the disc and shaft are listed in Tables 2–6.

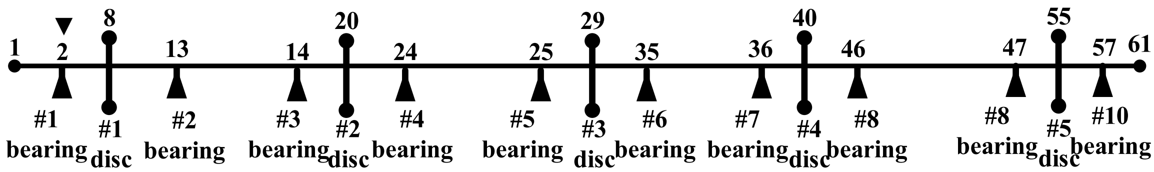

Figure 4. Five-span and five-disc rotor.

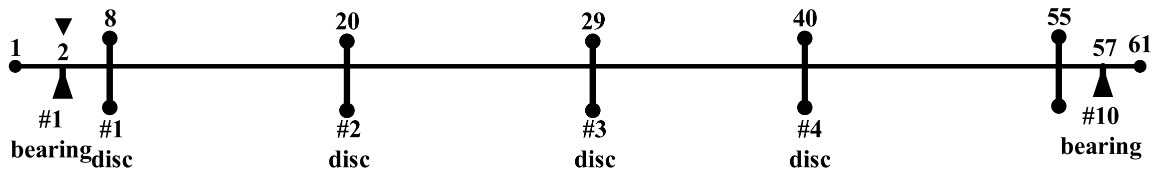

Figure 5. Single-span and five-disc rotor.

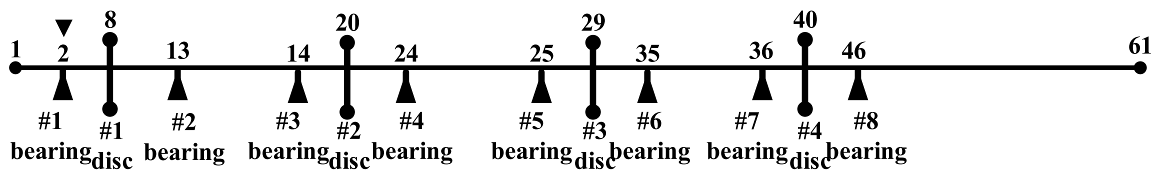

Figure 6. Four-span and four-disc rotor.

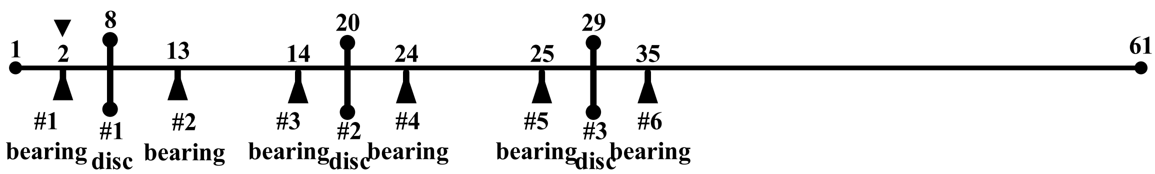

Figure 7. Three-span and three-disc rotor.

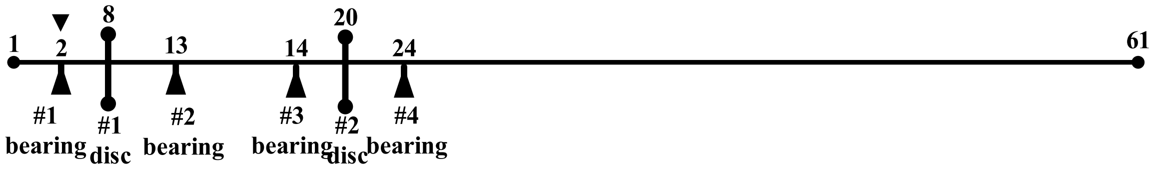

Figure 8. Two-span and two-disc rotor.

Figure 9. Single-span and single-disc rotor.

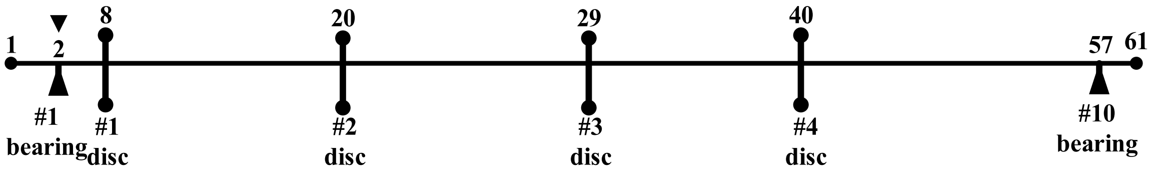

Figure 10. Single-span and four-disc rotor.

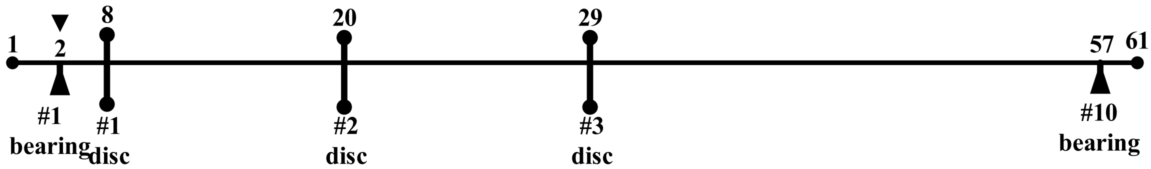

Figure 11. Single-span and three-disc rotor.

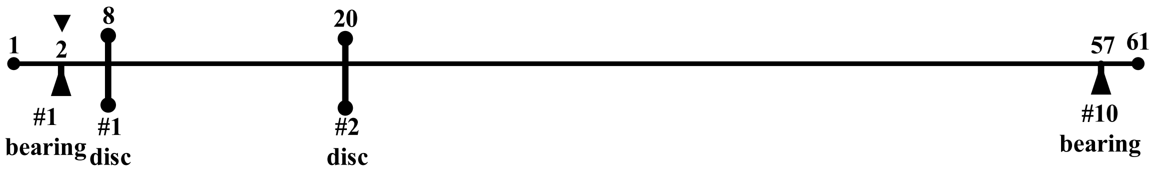

Figure 12. Single-span and two-disc rotor.

Table 2. Meanings of symbols in the computational example of the rotor.

Parameter	Meaning
r_shaft	Radius of the shaft
p_shaft	Density of the shaft
E_shaft	Elastic modulus of the shaft
L_shaft	Length of the shaft
r_disc	Radius of the disc
p_disc	Density of the disc
E_disc	Elastic modulus of the disc
L_disc	Width of the disc

Table 3. Parameters of the rotor shaft in the proposed computational examples.

Parameter	Value	Parameter	Value
r_shaft	10×10^{-3} m	L_shaft of h4.4, h1.4, g4.4, g1.4	$1800 \times 4 \times 10^{-3}$ m
p_shaft	7800 kg·m^{-3}	L_shaft of h3.3, h1.3, g3.3, g1.3	$1800 \times 3 \times 10^{-3}$ m
E_shaft	2.1×10^{11} Pa	L_shaft of h2.2, h1.2, g2.2, g1.2	$1800 \times 2 \times 10^{-3}$ m
L_shaft of h5.5, h1.5, g5.5, g1.5	$1800 \times 5 \times 10^{-3}$ m	L_shaft of h1.1, g1.1	$1800 \times 1 \times 10^{-3}$ m

Table 4. Parameters of the five eccentric disc in the proposed computational examples.

Parameter	Value	Parameter	Value	Parameter	Value
m_{1u}	0.05 kg	m_{2u}	0.15 kg	m_{3u}	0.01 kg
e_1	30×10^{-3} m	e_2	10×10^{-3} m	e_3	20×10^{-3} m
α_1	45°	α_2	90°	α_3	20°
Z_{1d}	Point 8	Z_{2d}	Point 20	Z_{3d}	Point 29
m_{4u}	0.10 kg	m_{5u}	0.05 kg	r_disc of #1~#5 disc	50×10^{-3} m
e_4	15×10^{-3} m	e_5	40×10^{-3} m	p_disc of of #1~#5 disc	7800 kg·m^{-3}
α_4	190°	α_5	290°	E_disc of of #1~#5 disc	2.1×10^{11} Pa
Z_{4d}	Point 40	Z_{5d}	Point 55	L_disc of of #1~#5 disc	10×10^{-3} m

Table 5. Parameters of the ten oil-journal bearings in the proposed computational examples.

Parameter	Value	Parameter	Value
$\begin{bmatrix} k_{1\cdot xx} & k_{1\cdot xy} \\ k_{1\cdot yx} & k_{1\cdot yy} \end{bmatrix}$	$\begin{bmatrix} 9\times10^6 & 10\times10^6 \\ -6\times10^6 & 4\times10^6 \end{bmatrix}$ N/m	$\begin{bmatrix} k_{2\cdot xx} & k_{2\cdot xy} \\ k_{2\cdot yx} & k_{2\cdot yy} \end{bmatrix}$	$\begin{bmatrix} 30\times10^6 & 6\times10^6 \\ -15\times10^6 & 10\times10^6 \end{bmatrix}$ N/m
$\begin{bmatrix} c_{1\cdot xx} & c_{1\cdot xy} \\ c_{1\cdot yx} & c_{1\cdot yy} \end{bmatrix}$	$\begin{bmatrix} 1\times10^5 & -6\times10^5 \\ -6\times10^5 & 10\times10^5 \end{bmatrix}$ N·s/m	$\begin{bmatrix} c_{2\cdot xx} & c_{2\cdot xy} \\ c_{2\cdot yx} & c_{2\cdot yy} \end{bmatrix}$	$\begin{bmatrix} 6\times10^5 & -14\times10^5 \\ -14\times10^5 & 15\times10^5 \end{bmatrix}$ N·s/m
$\begin{bmatrix} k_{3\cdot xx} & k_{3\cdot xy} \\ k_{3\cdot yx} & k_{3\cdot yy} \end{bmatrix}$	$\begin{bmatrix} 40\times10^6 & 7\times10^6 \\ -16\times10^6 & 11\times10^6 \end{bmatrix}$ N/m	$\begin{bmatrix} k_{4\cdot xx} & k_{4\cdot xy} \\ k_{4\cdot yx} & k_{4\cdot yy} \end{bmatrix}$	$\begin{bmatrix} 45\times10^6 & 9\times10^6 \\ -20\times10^6 & 14\times10^6 \end{bmatrix}$ N/m
$\begin{bmatrix} c_{3\cdot xx} & c_{3\cdot xy} \\ c_{3\cdot yx} & c_{3\cdot yy} \end{bmatrix}$	$\begin{bmatrix} 7\times10^5 & -15\times10^5 \\ -15\times10^5 & 16\times10^5 \end{bmatrix}$ N·s/m	$\begin{bmatrix} c_{4\cdot xx} & c_{4\cdot xy} \\ c_{4\cdot yx} & c_{4\cdot yy} \end{bmatrix}$	$\begin{bmatrix} 10\times10^5 & -20\times10^5 \\ -20\times10^5 & 20\times10^5 \end{bmatrix}$ N·s/m
$\begin{bmatrix} k_{5\cdot xx} & k_{5\cdot xy} \\ k_{5\cdot yx} & k_{5\cdot yy} \end{bmatrix}$	$\begin{bmatrix} 50\times10^6 & 15\times10^6 \\ -25\times10^6 & 20\times10^6 \end{bmatrix}$ N/m	$\begin{bmatrix} k_{6\cdot xx} & k_{6\cdot xy} \\ k_{6\cdot yx} & k_{6\cdot yy} \end{bmatrix}$	$\begin{bmatrix} 9\times10^6 & 10\times10^6 \\ -6\times10^6 & 10\times10^6 \end{bmatrix}$ N/m
$\begin{bmatrix} c_{5\cdot xx} & c_{5\cdot xy} \\ c_{5\cdot yx} & c_{5\cdot yy} \end{bmatrix}$	$\begin{bmatrix} 20\times10^5 & -30\times10^5 \\ -30\times10^5 & 30\times10^5 \end{bmatrix}$ N·s/m	$\begin{bmatrix} c_{6\cdot xx} & c_{6\cdot xy} \\ c_{6\cdot yx} & c_{6\cdot yy} \end{bmatrix}$	$\begin{bmatrix} 1\times10^5 & -6\times10^5 \\ -6\times10^5 & 10\times10^5 \end{bmatrix}$ N·s/m
$\begin{bmatrix} k_{7\cdot xx} & k_{7\cdot xy} \\ k_{7\cdot yx} & k_{7\cdot yy} \end{bmatrix}$	$\begin{bmatrix} 30\times10^6 & 6\times10^6 \\ -15\times10^6 & 10\times10^6 \end{bmatrix}$ N/m	$\begin{bmatrix} k_{8\cdot xx} & k_{8\cdot xy} \\ k_{8\cdot yx} & k_{8\cdot yy} \end{bmatrix}$	$\begin{bmatrix} 40\times10^6 & 7\times10^6 \\ -16\times10^6 & 11\times10^6 \end{bmatrix}$ N/m
$\begin{bmatrix} c_{8\cdot xx} & c_{8xy} \\ c_{8\cdot yx} & c_{8\cdot yy} \end{bmatrix}$	$\begin{bmatrix} 6\times10^5 & -14\times10^5 \\ -14\times10^5 & 15\times10^5 \end{bmatrix}$ N·s/m	$\begin{bmatrix} c_{8\cdot xx} & c_{8\cdot xy} \\ c_{8\cdot yx} & c_{8\cdot yy} \end{bmatrix}$	$\begin{bmatrix} 7\times10^5 & -15\times10^5 \\ -15\times10^5 & 16\times10^5 \end{bmatrix}$ N·s/m
$\begin{bmatrix} k_{9\cdot xx} & k_{9\cdot xy} \\ k_{9\cdot yx} & k_{9\cdot yy} \end{bmatrix}$	$\begin{bmatrix} 45\times10^6 & 9\times10^6 \\ -20\times10^6 & 14\times10^6 \end{bmatrix}$ N/m	$\begin{bmatrix} k_{10\cdot xx} & k_{10\cdot xy} \\ k_{10\cdot yx} & k_{10\cdot yy} \end{bmatrix}$	$\begin{bmatrix} 50\times10^6 & 15\times10^6 \\ -25\times10^6 & 20\times10^6 \end{bmatrix}$ N/m
$\begin{bmatrix} c_{9\cdot xx} & c_{9\cdot xy} \\ c_{9\cdot yx} & c_{9\cdot yy} \end{bmatrix}$	$\begin{bmatrix} 10\times10^5 & -20\times10^5 \\ -20\times10^5 & 20\times10^5 \end{bmatrix}$ N·s/m	$\begin{bmatrix} c_{10\cdot xx} & c_{10\cdot xy} \\ c_{10\cdot yx} & c_{10\cdot yy} \end{bmatrix}$	$\begin{bmatrix} 20\times10^5 & -30\times10^5 \\ -30\times10^5 & 30\times10^5 \end{bmatrix}$ N·s/m
Z_{1b}	Point 2	Z_{2b}	Point 13
Z_{3b}	Point 14	Z_{4b}	Point 24
Z_{5b}	Point 25	Z_{6b}	Point 35
Z_{7b}	Point 36	Z_{8b}	Point 46
Z_{9b}	Point 47	Z_{10b}	Point 57

Table 6. Parameters of the ten rolling bearings in the proposed computational examples.

Z_{1b}	Z_{2b}	Z_{3b}	Z_{4b}	Z_{5b}	Z_{6b}	Z_{7b}	Z_{8b}
Point 2	Point 13	Point 14	Point 24	Point 25	Point 35	Point 36	Point 46
Z_{9b}	Z_{10b}	$\begin{bmatrix} k_{i\cdot xx} & k_{i\cdot xy} \\ k_{i\cdot yx} & k_{i\cdot yy} \end{bmatrix}$, $i = 1$ to 10			$\begin{bmatrix} c_{i\cdot xx} & c_{i\cdot xy} \\ c_{i\cdot yx} & c_{i\cdot yy} \end{bmatrix}$, $i = 1$ to 10		
Point 47	Point 57	$\begin{bmatrix} 9\times10^6 & 0 \\ 0 & 8.9\times10^6 \end{bmatrix}$ N/m			$\begin{bmatrix} 80 & 0 \\ 0 & 75 \end{bmatrix}$ N·s/m		

Based on the CRDAM, FEM [10] and Ricatti [11] methods, a calculation program to calculate the unbalance responses is developed using Matlab software. As shown in Figures 4–12, the rotor-shaft is divided into 60 unit elements of equal length and the discs and bearings are lumped when unbalance responses of FEM and Ricatti methods are calculated by the program. The #2 (2th) point's unbalance responses changed with the rotating frequencies (speeds) are obtained for the comparison among the three methods. In the computation, the calculating frequency is from 0 to 1000 Hz and the interval is 1 Hz.

3.2. Calculated Critical Frequencies

3.2.1. Results

Tables A1–A9, in which the values of critical frequencies calculated by CRDAM, FEM and Ricatti are listed, are obtained in Appendix A. By treating FEM as the base-exact, C/F and R/F are used to compare the discrepancies among the three methods. C/F is the relative error of critical frequency calculated by CDRAM to the frequency obtained by FEM and R/F represents the relative error of critical frequency calculated by Ricatti to the frequency calculated by FEM.

According to the two Tables, the critical frequency values calculated by the three methods are almost equal. For g1.1, the maximum values of C/F and R/F are 0.852% and 2.273%, respectively. For g2.2, g3.3, g4.4, g5.5, g1.2, g1.3, g1.4 and g1.5, they are 0.129% and 0.528%, 1.310% and 5.022%, 0.570% and 3.422%, 0.294% and 2.941%, 0.422% and 1.582%, 0.474% and 2.966%, 0.262% and 2.345%, 0.333% and 2.333%, respectively. For the rotors supported by oil journal bearings h1.1, h2.2, h3.3, h4.4, h5.5, h1.2, h1.3, h1.4 and h1.5, they are 0.168% and 0.168%, 0.125% and 0.526%, 1.392% and 5.139%, 0.565% and 3.578%, 0.830% and 3.271%, 0.521% and 1.771%, 0.590% and 3.066%, 0.529% and 2.340%, 0.000% and 2.326%, respectively. These maximum values of the relative errors are quite small.

3.2.2. Discussion

Figures 13 and 14, which indicate the difference of the critical frequency calculated by CRDAM, FEM and Ricatti, are obtained using the data of C/F and R/F in Tables A1–A9.

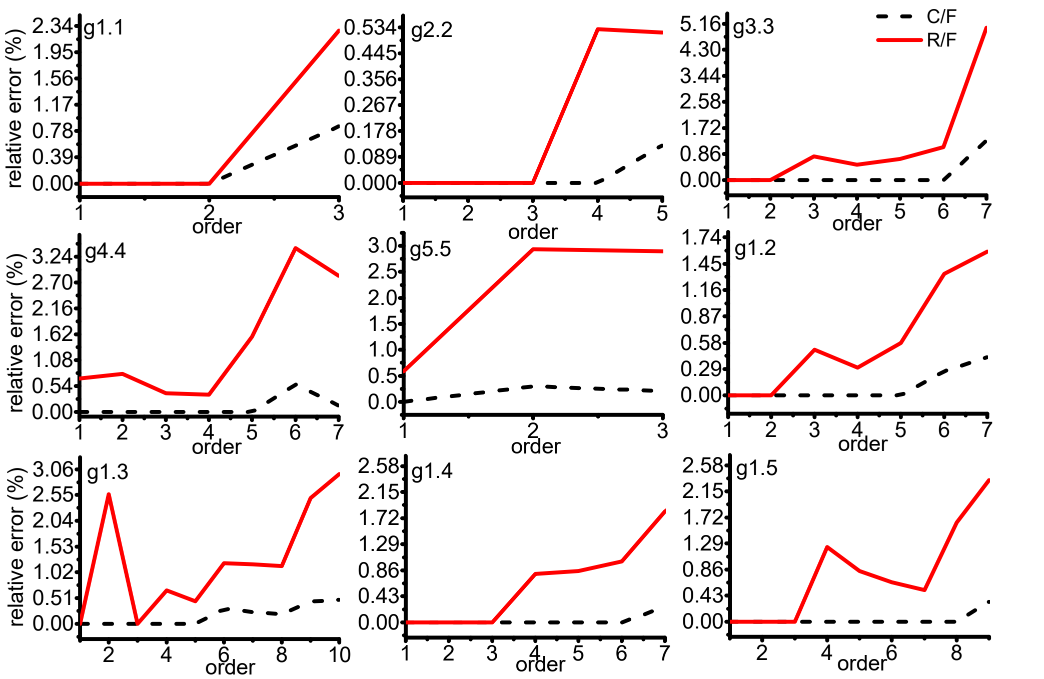

Figure 13. Relative error of calculated critical frequency of CDRAM to FEM and Ricatti to FEM when the rotor is supported by rolling bearings.

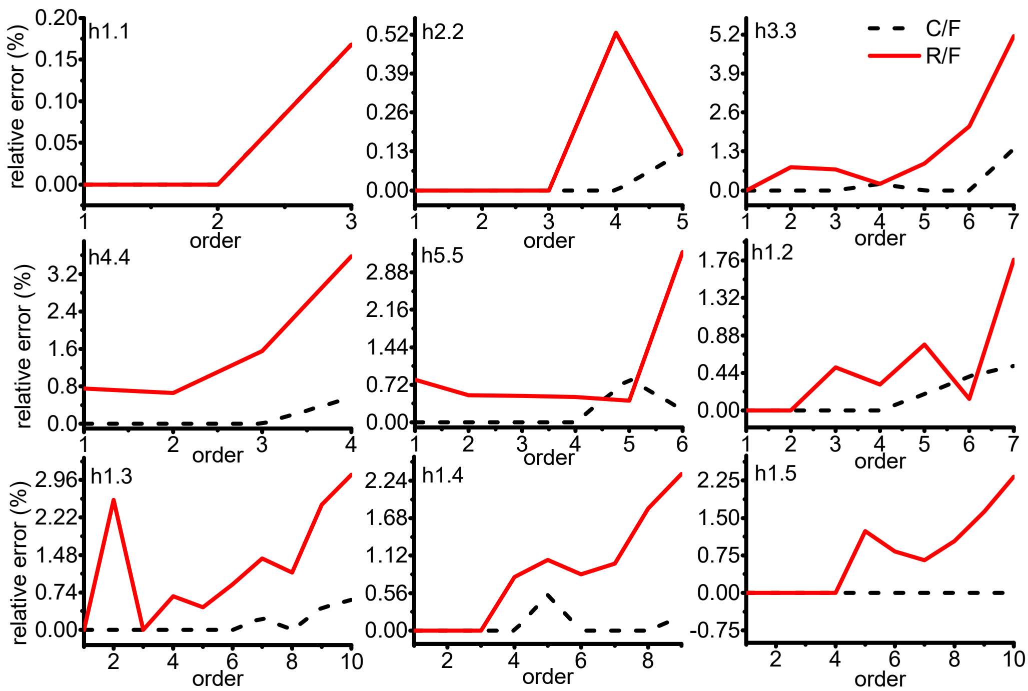

Figure 14. Relative error of calculated critical frequency of CDRAM to FEM and Ricatti to FEM when the rotor is supported by oil journal bearings.

According to Figures 13 and 14, the low order critical frequencies calculated by the three methods are almost equal. The difference becomes bigger among the high order critical frequencies. Moreover, the higher the order, the greater the difference except the value of R/F in g1.3 and h1.3. For h1.1, C/F curve and R/F curve coincide. For the other rotors, C/F cure is below R/F curve. It indicates that the critical frequency calculated by CRDAM is closer to the critical frequency calculated by FEM than the critical frequency calculated by Ricatti. Even at high order critical frequency, the difference between the critical frequency calculated by FEM and the critical frequency calculated by CRDAM are small. It can be inferred that the proposed CRDAM method is closer to FEM than Ricatti.

3.3. Calculated Unbalance Response

3.3.1. Results

Based on CRDAM, FEM and Ricatti, three curves, which represent the relation between unbalance responses and rotating frequencies, are obtained in Figure 15. They are calculated at #2 point of the computational example g3.3.

According to Figure 15, it is found that the three obtained curves have the same trend. According to Figure 15a,b, the three curves, which are obtained from 0 to 50 Hz and 50 to 150 Hz, are well coincident. It is because that the first and second order critical frequencies are equal. However, from 150 to 400 Hz, the three curves are not well coincident. The unbalance response curves obtained by CRDAM and FEM coincide better than the curve obtained by Ricatti according to Figure 15c. According to Figure 15d,e, the curves obtained by CRDAM and FEM still coincide better from 300 Hz to 600 Hz than the curve obtained by Ricatti. The reason is that the values of the critical frequencies calculated by CRDAM and FEM coincide better than the value calculated by Ricatti. According to Figure 15f, the three curves from 600 to 1000 Hz are not well coincident near the seventh order critical frequency due to the difference of the seventh order critical frequency. However, the three curves are well coincident when the calculating frequencies are far from the seventh critical frequency.

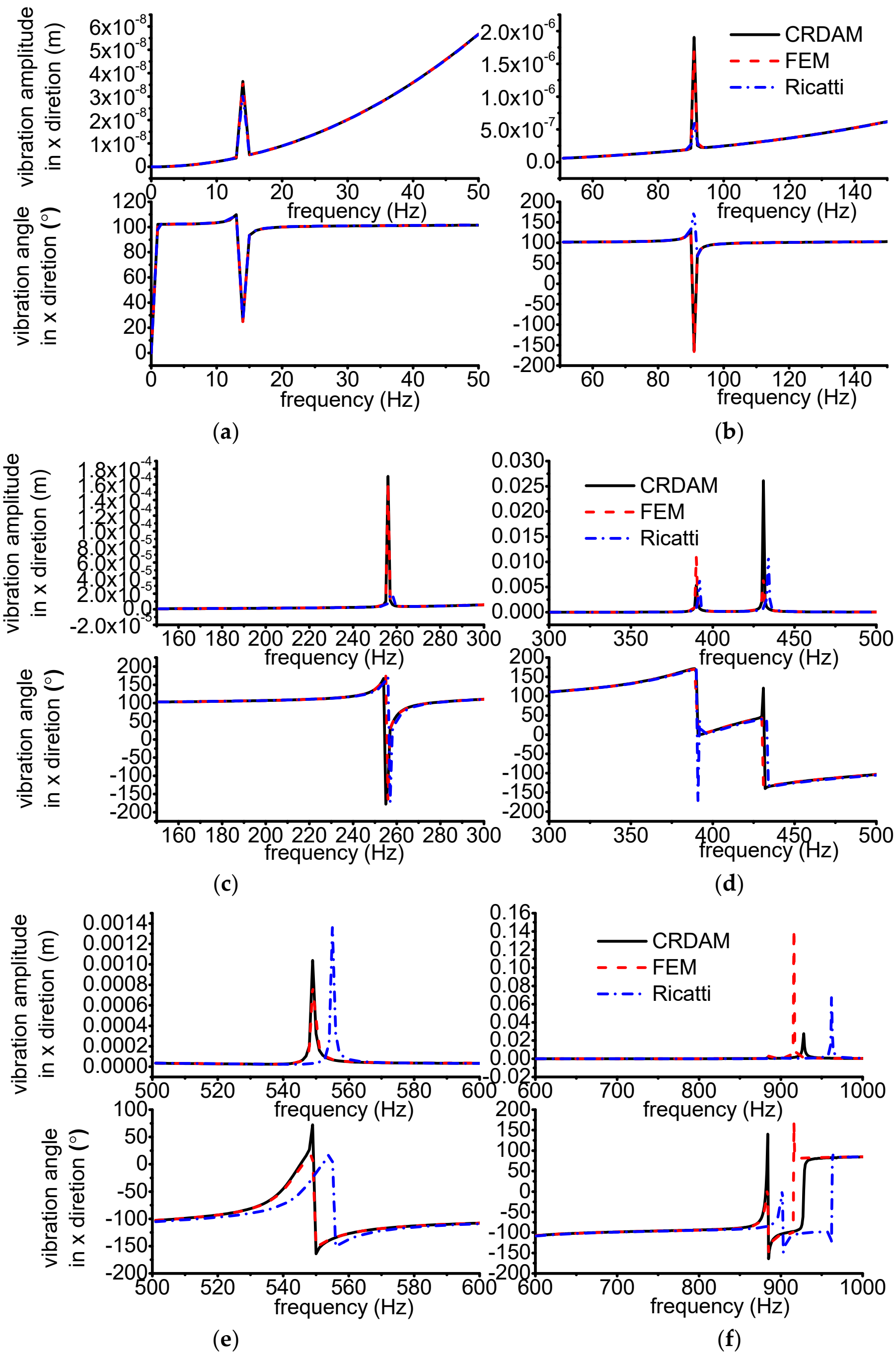

Figure 15. Calculated unbalance response of point #2 of g3.3: (**a**) 0~50 Hz; (**b**) 50~150 Hz; (**c**) 150~300 Hz; (**d**) 300~500 Hz; (**e**) 500~600 Hz; (**f**) 600~1000 Hz.

Moreover, similar phenomena can be found in simulations of the computational examples g1.1, g2.2, g1.2, g1.3, h1.1, h2.2, h3.3, h1.2, h1.3 g5.5, g1.4, g1.5, h4.4, h5.5, h1.4 and h1.5 whose results are shown in Figures A1–A16 in Appendix C.

Figure 16 shown the three curves of relation between unbalance responses and rotating frequencies is obtained using the computational example g4.4. The three obtained curves have the same trend. However, according to Figure 16a, although the first order frequency values are almost equal, the three unbalance response curves are not well coincident near the first order critical frequency. The peak value of FEM amplitude curve is biggest. However, the three curves coincide well when the calculating frequencies are far away from the first order critical frequency.

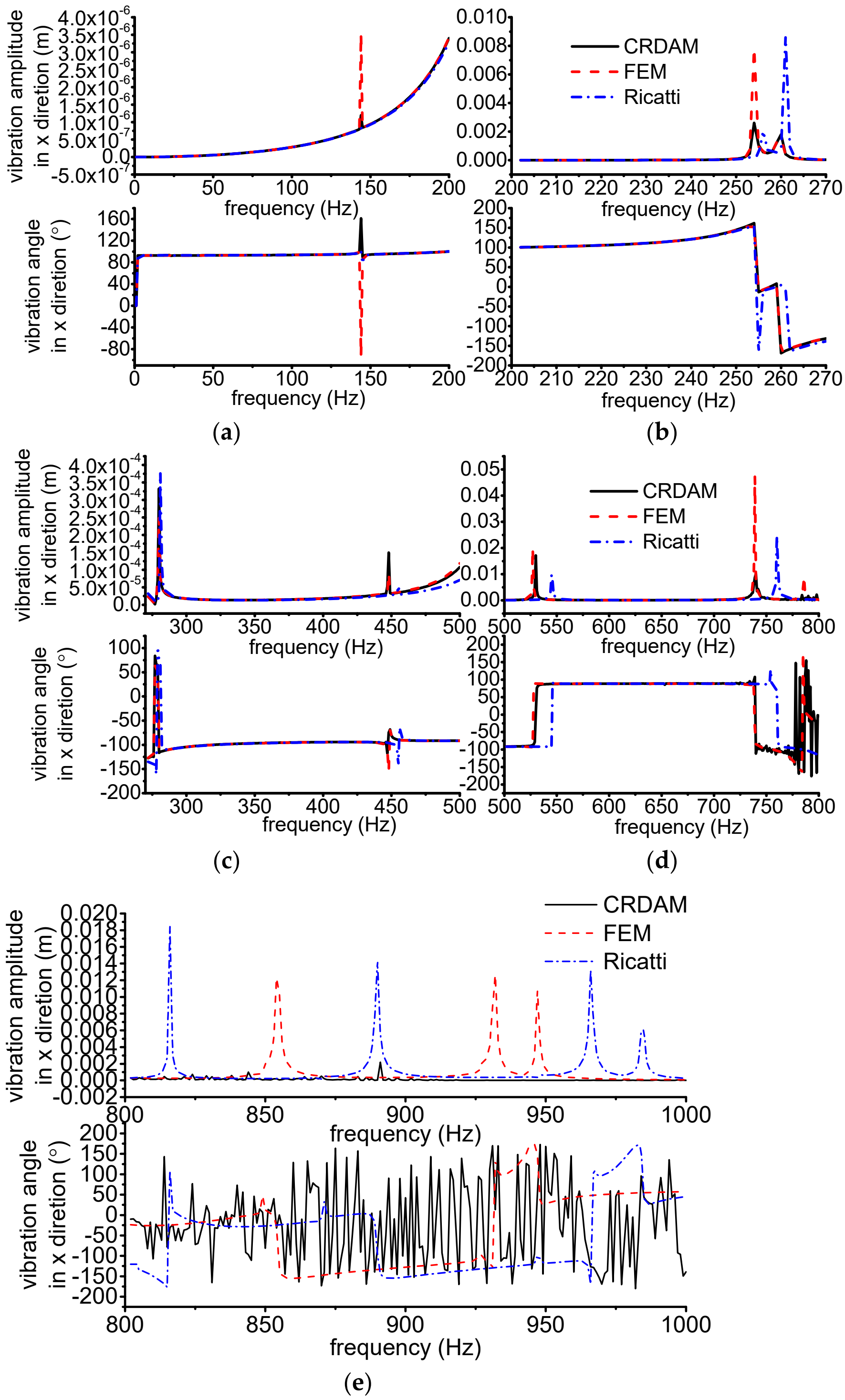

Figure 16. Calculated unbalance response of point #2 of g4.4: (**a**) 0~200 Hz; (**b**) 200~270 Hz; (**c**) 270~500 Hz; (**d**) 500~800 Hz; (**e**) 800~1000 Hz.

According to Figure 16b, the three curves from 200 to 270 Hz are well coincident except near the second and third critical frequency. Since the second and third order critical frequency values calculated by CRDAM and FEM are equal, the two curves obtained by CRDAM and FEM coincide better than the curve obtained by Ricatti at the two critical frequencies. At the second order frequency, the peak value of FEM amplitude curve is the biggest. At the third order frequency, the peak value of Ricatti amplitude curve is the biggest.

According to Figure 16c, the three curves from 270 to 500 Hz are still well coincident except near the fourth and fifth order critical frequency. The two curves obtained by CRDAM and FEM coincide better than the curve obtained by Ricatti at the two critical frequencies. According to Figure 16d, the curve obtained by CRDAM is well coincident with the curve obtained by FEM when the frequency is smaller than the seventh order critical frequency. It is also coincident with the curve obtained by Ricatti when the frequency is far away from the sixth and seventh order critical frequency. While from the seventh order critical frequency to 800 Hz, the curve obtained by CRDAM does not coincide with the two curves obtained by FEM and Ricatti at all.

However, according to Figure 16e, the curve obtained by CRDAM is obviously not coincident with the two curves obtained by FEM and Ricatti. From the angle curve obtained by CRDAM, the angle changes frequently and suddenly from positive to negative with frequency, but the phenomenon does not occur on the angle curve obtained by FEM and Ricatti. It is indicated that numerical instability of CRDAM occurs and the unbalance response cannot be correctly calculated by the proposed method from the seventh order critical frequency to 1000 Hz. While for the FEM and Ricatti methods, there is no numerical instability phenomenon although the two curve obtained by them are not coincident obviously from the seventh order critical frequency to 1000 Hz.

3.3.2. Discussion

(1) Accuracy

From the above, the three unbalance response curves calculated by CRDAM, FEM and Ricatti are well coincident when the frequency is away from the critical frequency, but they are different when the frequency is near the critical frequency. At the critical frequency, the peak value of the amplitude of unbalance response curve appears and the amplitude decreases or increases rapidly near the critical frequency. When the peak values are different, the three unbalance response curves are not well coincident. When the same order critical frequencies are different, their coincidence becomes worse. The severity of the inconsistency of the unbalanced response is positively correlated with the difference of the critical frequency calculated the three methods.

However, the three unbalance response curves calculated by three methods are well coincident when the frequency is smaller than the low order frequency (first, second, third and fourth order). Even near the lower critical frequency, the three unbalance response curves calculated by the three methods coincide well. The reason is that the low order frequencies and the unbalance response amplitude calculated by the three methods are almost equal.

To intuitively evaluate the coincidence of the three unbalance response curves calculated by the three methods, Figures 17 and 18 are obtained using the computational example h5.5 and h1.5, respectively. In Figures 17 and 18, the red curve represents the error of CRDAM to FEM and the black curve represents the error of CRDAM to FEM. The relative error is used to describe the amplitude error of unbalance responses and the absolute error is used to describe the angle error.

According to Figure 17a–c, the red curve is below the black curve from 0 Hz to 300 Hz, which means that the error of FEM to CRDAM is smaller than the error of Ricatti to CRDAM. The unbalance response obtained by CRDAM is closer to the unbalance response obtained by FEM than the unbalance response obtained by Ricatti. The errors are smaller when the frequency is away from the first, second, third, fourth and fifth critical frequency than when near these critical frequency. The error of FEM to CRDAM is small even when the frequency is near these critical frequency. The similar results can also be obtained from Figure 18a–c.

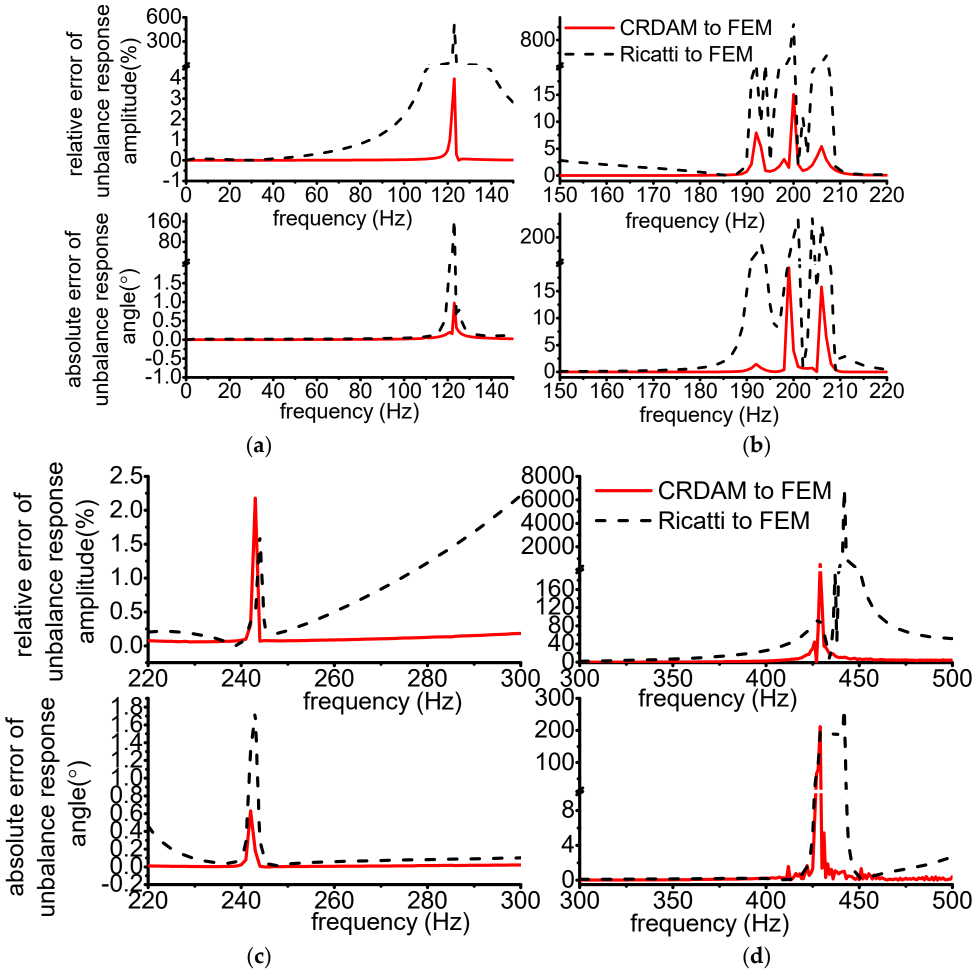

Figure 17. Relative error of #2 point's unbalance response amplitude and absolute error of #2 point's unbalance response angle: (**a**) 0~150 Hz; (**b**) 150~220 Hz; (**c**) 220~300 Hz; (**d**) 300~500 Hz.

According to Figure 17e, the red curve is close to the black curve when the frequency is smaller than the sixth order critical frequency. When the frequency is higher than the sixth order critical frequency, most parts of the red curve is above the black curve, but there are some parts of the red curve and black curve are coincident and there are some parts of the red curve is above the black curve. Hence, it can also be inferred that the unbalance response obtained by CRDAM is closer to the unbalance response obtained by FEM than the unbalance response obtained by Ricatti. Moreover, the errors are bigger when the frequency is near the sixth order critical frequency than when the frequency is away from the sixth order critical frequency. The similar results can also be obtained from Figure 18d–h.

From the above, the unbalance responses calculated by the CRDAM, FEM and Ricatti are different. The unbalance response obtained by CRDAM is closer to the unbalance response obtained by FEM than the unbalance response obtained by Ricatti, especially when the frequency is smaller than the low order frequencies. Their differences are small when the frequency is away from the critical frequency and the differences are big when near these critical frequencies. When the frequency is smaller than the low order frequency, their differences are small too.

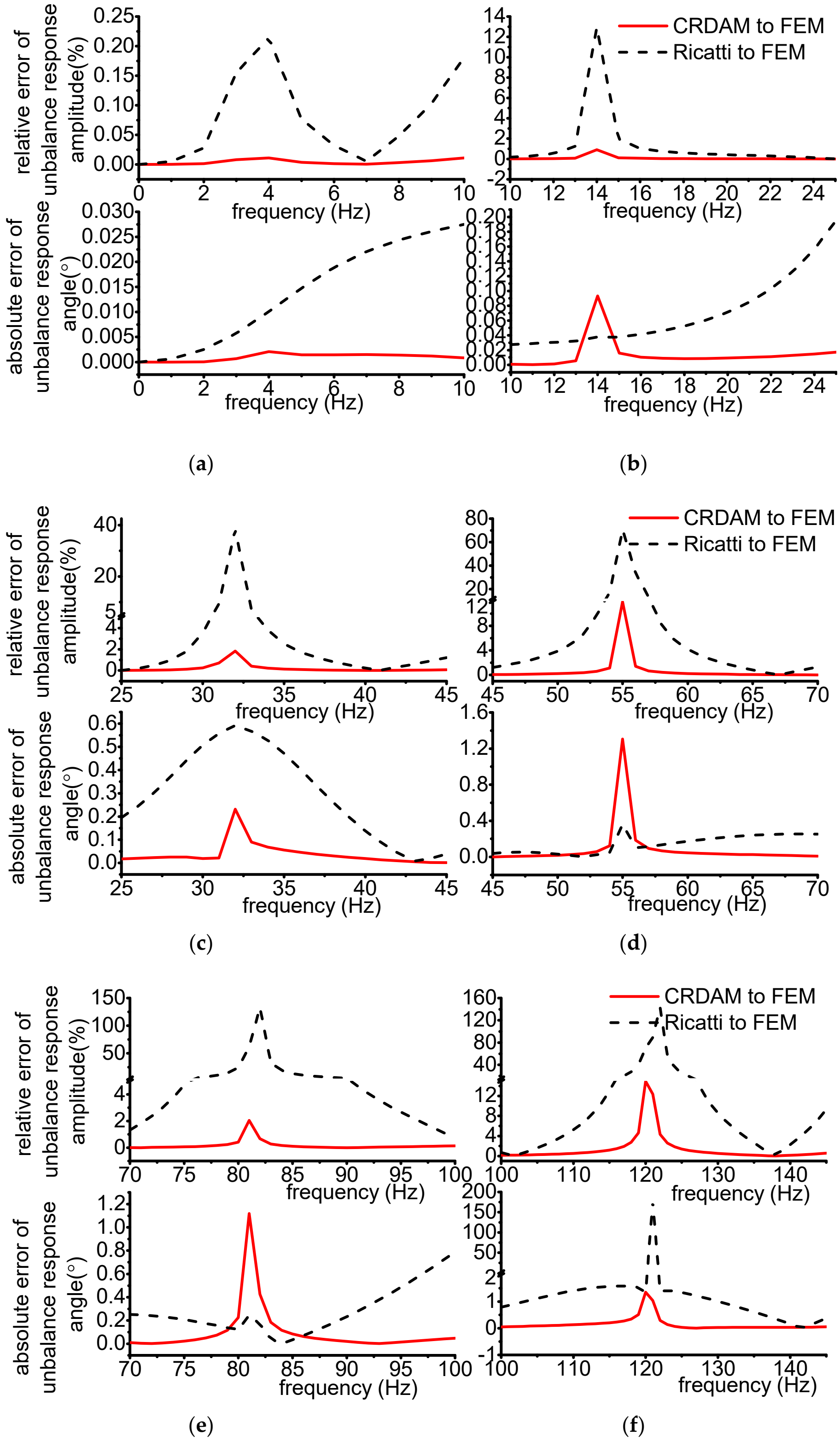

Figure 18. *Cont.*

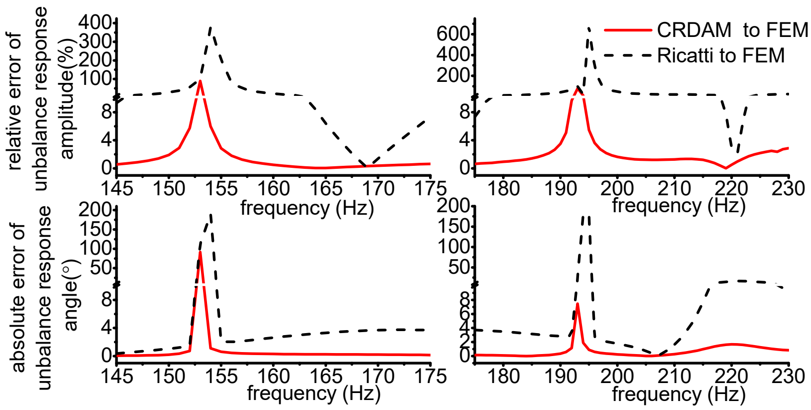

(**g**) (**h**)

Figure 18. Relative error of #2 point's unbalance response amplitude and absolute error of #2 point's unbalance response angle: (**a**) 0~10 Hz; (**b**) 10~25 Hz; (**c**) 25~45 Hz; (**d**) 45~70 Hz; (**e**) 70~100 Hz; (**f**) 100~145 Hz; (**g**) 145~175 Hz; (**h**) 175~230 Hz.

In addition, for Ricatti method, the rotor is simplified as a beam mode with lumped mass, which causes errors in modelling and the inaccuracy of calculating unbalance response. While for FEM, the model is closer to real rotors and unbalance responses obtained by FEM are more accuracy than Ricatti method because the factors such as moment of inertia, gyroscopic moment and shear deformation are considered. CRDAM is closer to FEM than Ricatti. Hence, CRDAM can be considered as an effective method for calculating unbalance responses of rotors.

According to the above conclusion, the unbalance responses of all points of g1.5 and g5.5 at the frequencies which are away from the critical frequencies, are obtained in Figures 19 and 20. For h1.5, the frequencies 1 Hz, 10 Hz, 25 Hz, 45 Hz, 65 Hz, 100 Hz, 130 Hz, 220 Hz, 180 Hz and 280 Hz are selected. For h5.5, they are 100 Hz, 300 Hz and 400 Hz.

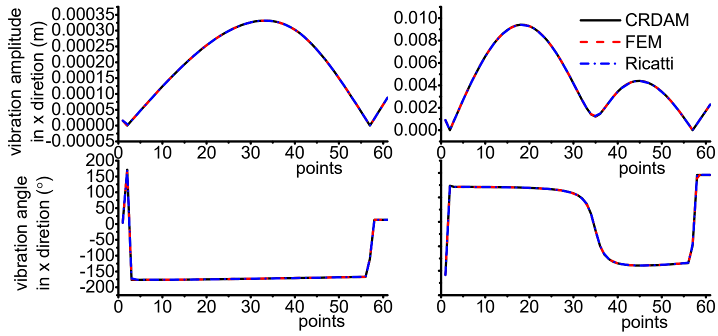

(**a**) (**b**)

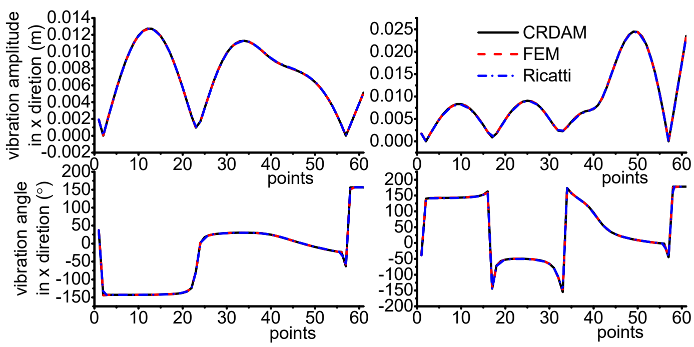

(**c**) (**d**)

Figure 19. *Cont.*

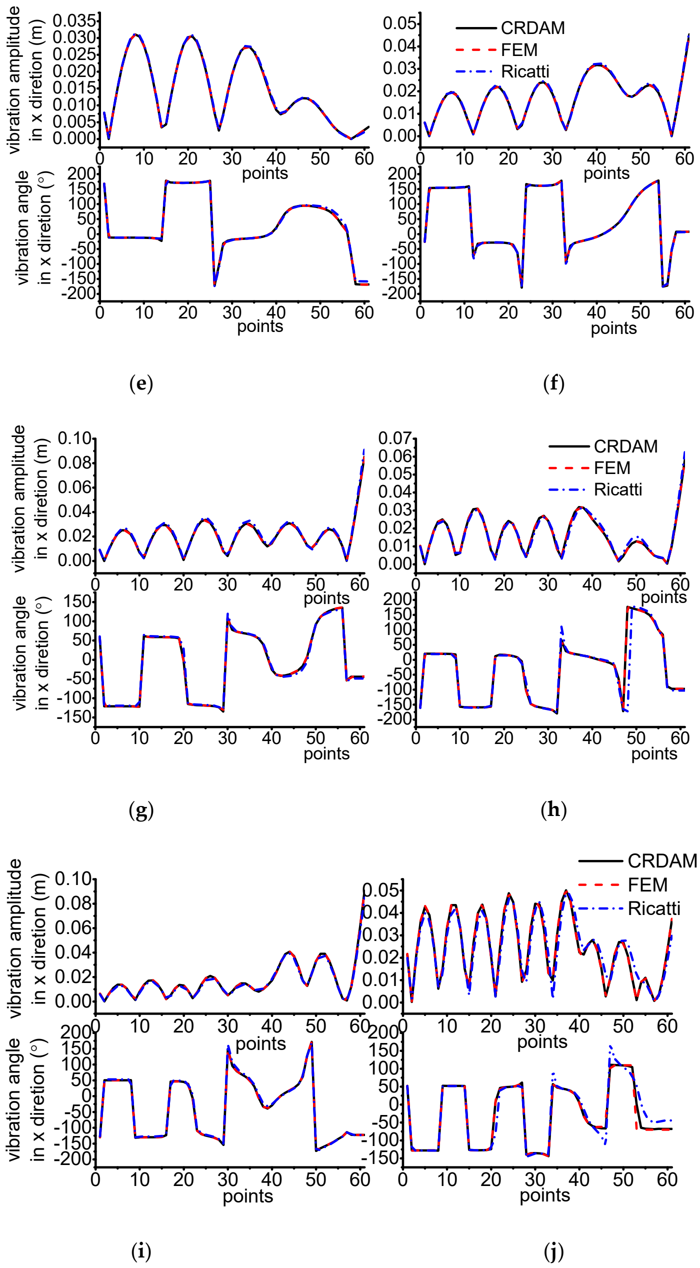

Figure 19. Calculated unbalance response of point #1–61 of g1.5 at ten fixed frequency: (**a**) 1 Hz; (**b**) 10 Hz; (**c**) 25 Hz; (**d**) 45 Hz; (**e**) 65 Hz; (**f**) 100 Hz; (**g**) 130 Hz; (**h**) 180 Hz; (**i**) 220 Hz; (**j**) 280 Hz.

According to Figure 19, it is found that using CRDAM, FEM and Ricatti, the three obtained curves, which represent the relation between unbalance responses and positions of the 61 points on the shaft at a fixed rotating frequency, are well coincident. The curve obtained by Ricatti are well coincident with the CRDAM and FEM curves when the frequency is 1 Hz, 10 Hz, 25 Hz, 45 Hz, 65 Hz, 100 Hz, 130 Hz and 220 Hz, but not well coincident with the two curves at 180 Hz and 280 Hz. According to Figure 19h, the curve obtained by Ricatti are not coincident with the other two curves at #48–49 points when the frequency is 180 Hz. According to Figure 19j, the curve obtained by Ricatti are not coincident with the other two curves at #34–35 and #45–56 points when the frequency is 280 Hz. According to Figure 20, the three obtained curves are still well coincident. According to Figure 20b,c, the curve obtained by CRDAM is better coincident with the curve obtained by FEM than the curve obtained by Ricatti. The curve obtained by Ricatti are not coincident with the other two curves at #58–59 points in Figure 20b and the curve obtained by Ricatti are not coincident with the other two curves at #11–12 points in Figure 20c. It indicates that the CRDAM method is closer to FEM than Ricatti.

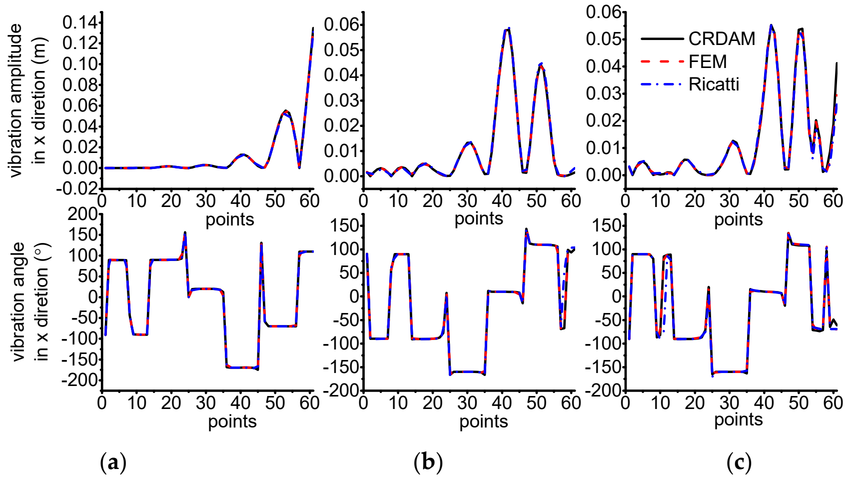

Figure 20. Calculated unbalance response of point #1~61 of g5.5 at three fixed frequency: (**a**) 100 Hz; (**b**) 300 Hz; (**c**) 400 Hz.

(2) Numerical stability

According to simulation of g4.4, unbalance response angle obtained by CRDAM changes frequently and suddenly from positive to negative with frequency when the frequency is high. It indicates that the numerical instability occurs and the unbalance response cannot be correctly calculated by the proposed method.

Moreover, similar phenomena can be found in simulations of g5.5, g1.4, g1.5, h4.4, h5.5, h1.4 and h1.5 whose results are shown in the Figures 21–27. According to Figure 21 obtained using g5.5, the phenomenon of numerical instability of CRDAM is obviously when the rotating frequency is higher than 800 Hz. According to Figure 22 obtained using g1.4, numerical instability of CRDAM occurs after 600 Hz and becomes more serious when the frequency increases. For g1.5, numerical instability of CRDAM occurs after 400 Hz and becomes more serious when the frequency increases according to Figure 23. For h4.4, the numerical instability occurs at 630 Hz and becomes obvious from 700 Hz to 1000 Hz according to Figure 24. According to Figure 25, numerical instability of CRDAM in h5.5 occurs after 500 Hz. According to Figure 26, it occurs after 580 Hz and becomes more serious from 650 Hz to 1000 Hz. According to Figure 27, it occurs after 400 Hz and becomes more serious from 500 Hz to 1000 Hz. Whereas for FEM and Ricatti, there is no numerical instability phenomenon although their curves still do not coincide according to Figures 16 and 21–27.

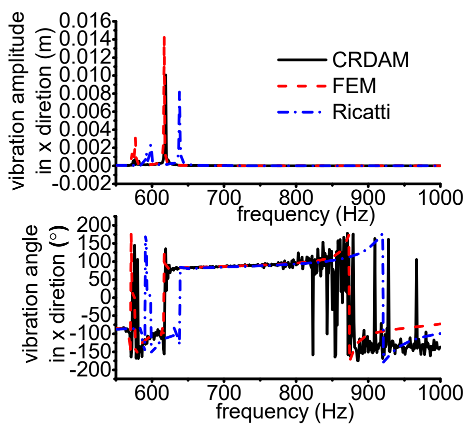

Figure 21. Calculated unbalance response of point #2 in g5.5 from 550 Hz to 1000 Hz.

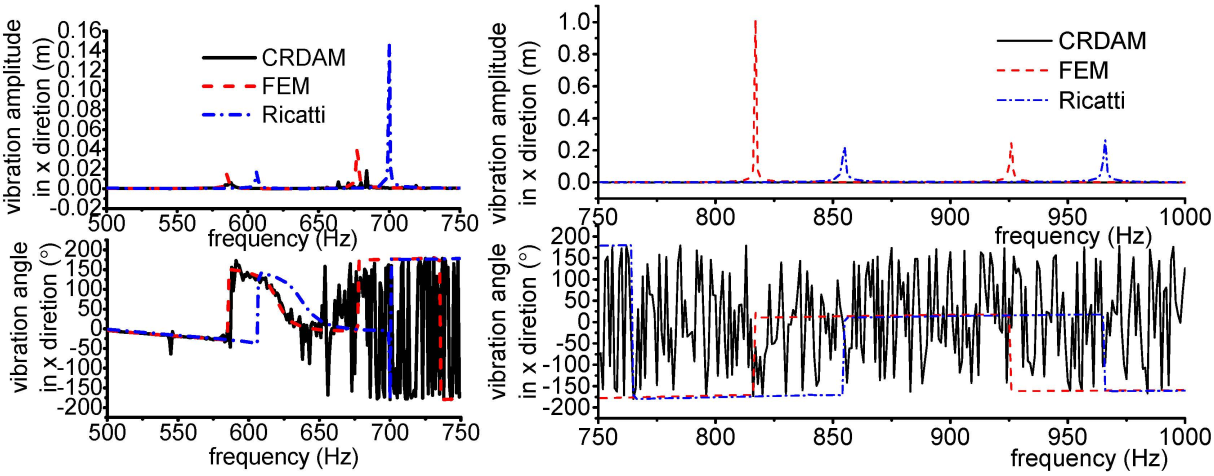

(**a**) (**b**)

Figure 22. Calculated unbalance response of point #2 in g1.4: (**a**) 500~750 Hz; (**b**) 750~1000 Hz.

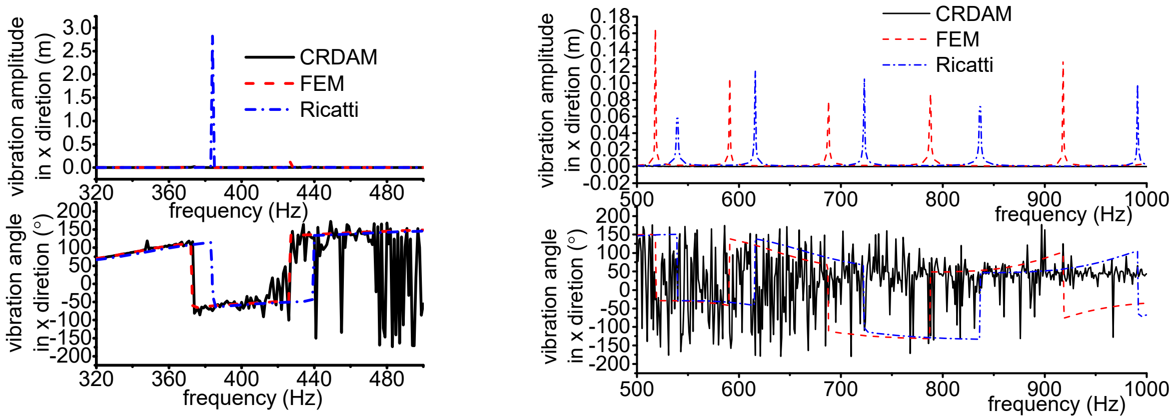

(**a**) (**b**)

Figure 23. Calculated unbalance response of point #2 in g1.5: (**a**) 320–500 Hz; (**b**) 500–1000 Hz.

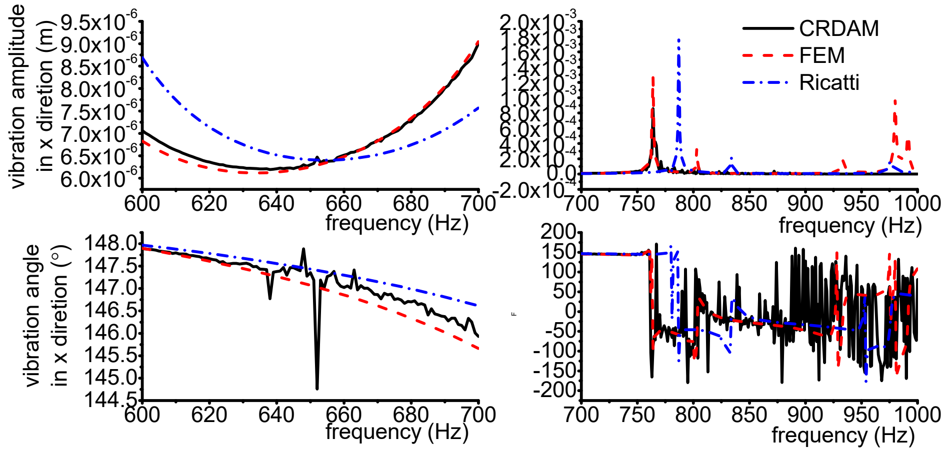

(**a**) (**b**)

Figure 24. Calculated unbalance response of point #2 in h4.4: (**a**) 600–700 Hz; (**b**) 700–1000 Hz.

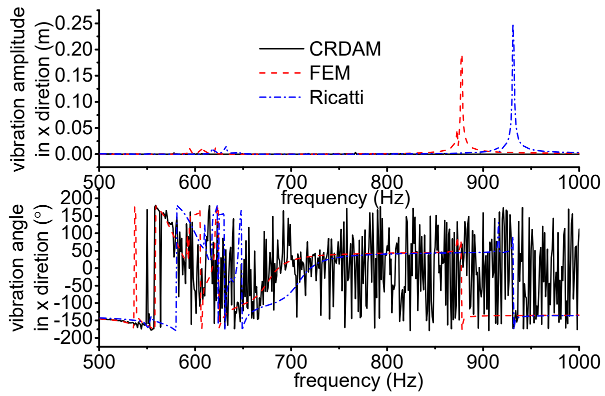

Figure 25. Calculated unbalance response of point #2 in h5.5 from 500 Hz to 1000 Hz.

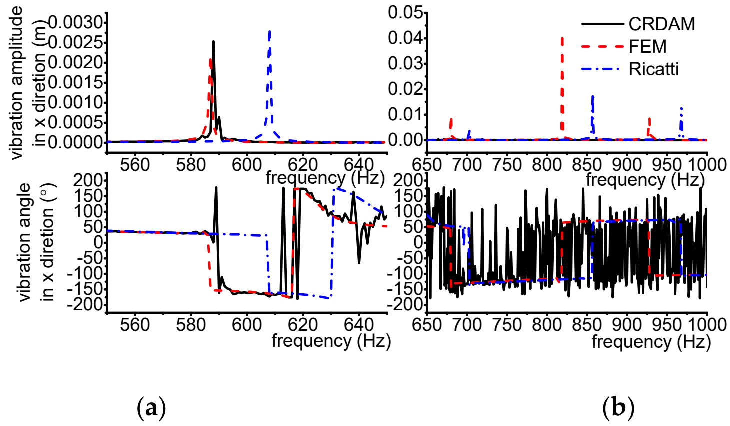

Figure 26. Calculated unbalance response of point #2 in h1.4: (**a**) 540~650 Hz; (**b**) 650~1000 Hz.

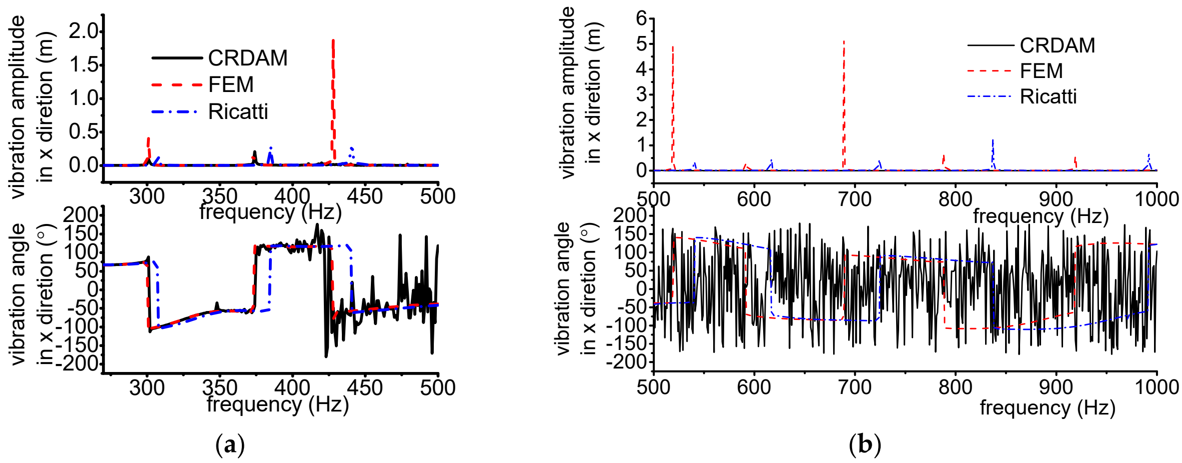

Figure 27. Calculated unbalance response of point #2 in h1.5: (**a**) 270~500 Hz; (**b**) 500~1000 Hz.

When Matlab performs inversion of the matrix M_{11} at some frequencies, the alarm that results may be inaccurate because M_{11} is close to singular or badly scaled occurs. Therefore, the reciprocal condition of a matrix is used to investigate the numerical stability which is caused by the singular matrix M_{11}. If a matrix is well conditioned, its reciprocal condition number is near 1. If a matrix is badly conditioned, its reciprocal condition is near 0. Figures 28–31 which show the reciprocal condition numbers of M_{11}, are obtained by the function round( ) of Matlab.

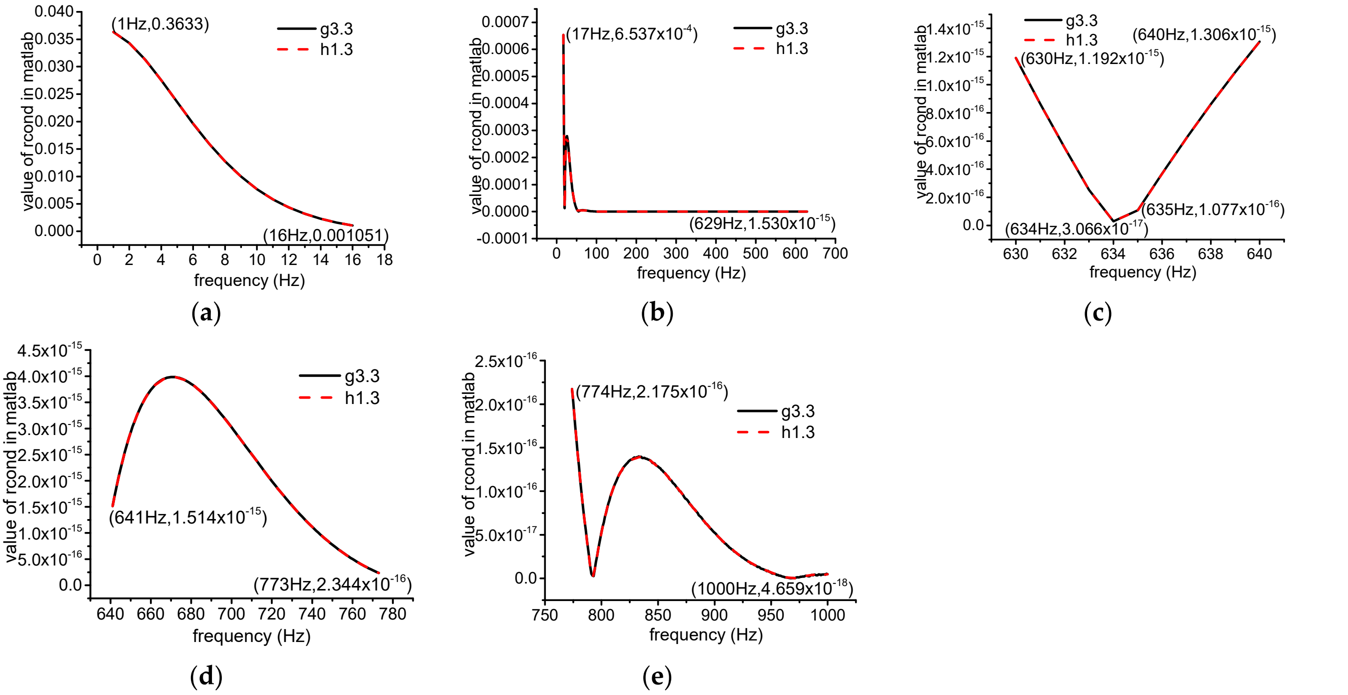

Figure 28. The reciprocal condition of the matrix M_{11}: (**a**) 1~16 Hz; (**b**) 17~629 Hz; (**c**) 630~640 Hz; (**d**) 640~773 Hz; (**e**) 774~1000 Hz.

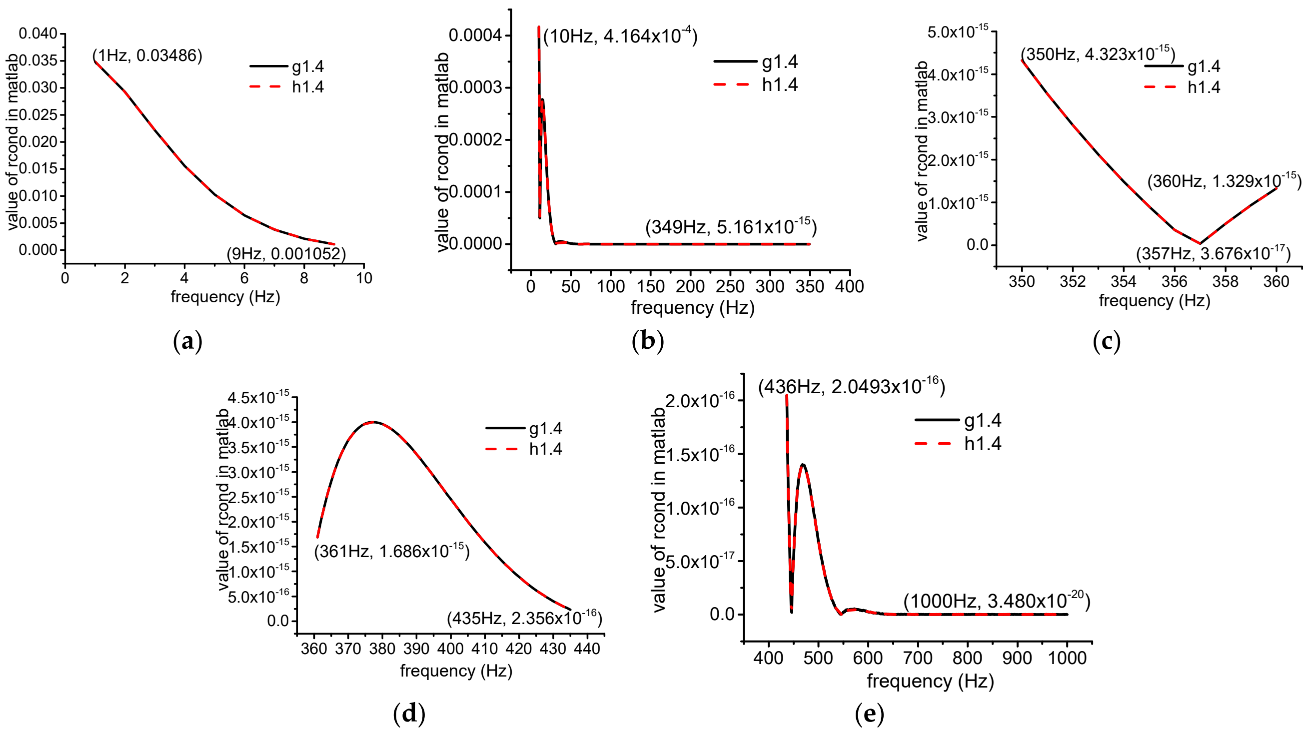

Figure 29. The reciprocal condition of the matrix M_{11}: (**a**) 1~9 Hz; (**b**) 10~349 Hz; (**c**) 350~360 Hz; (**d**) 361~435 Hz; (**e**) 436~1000 Hz.

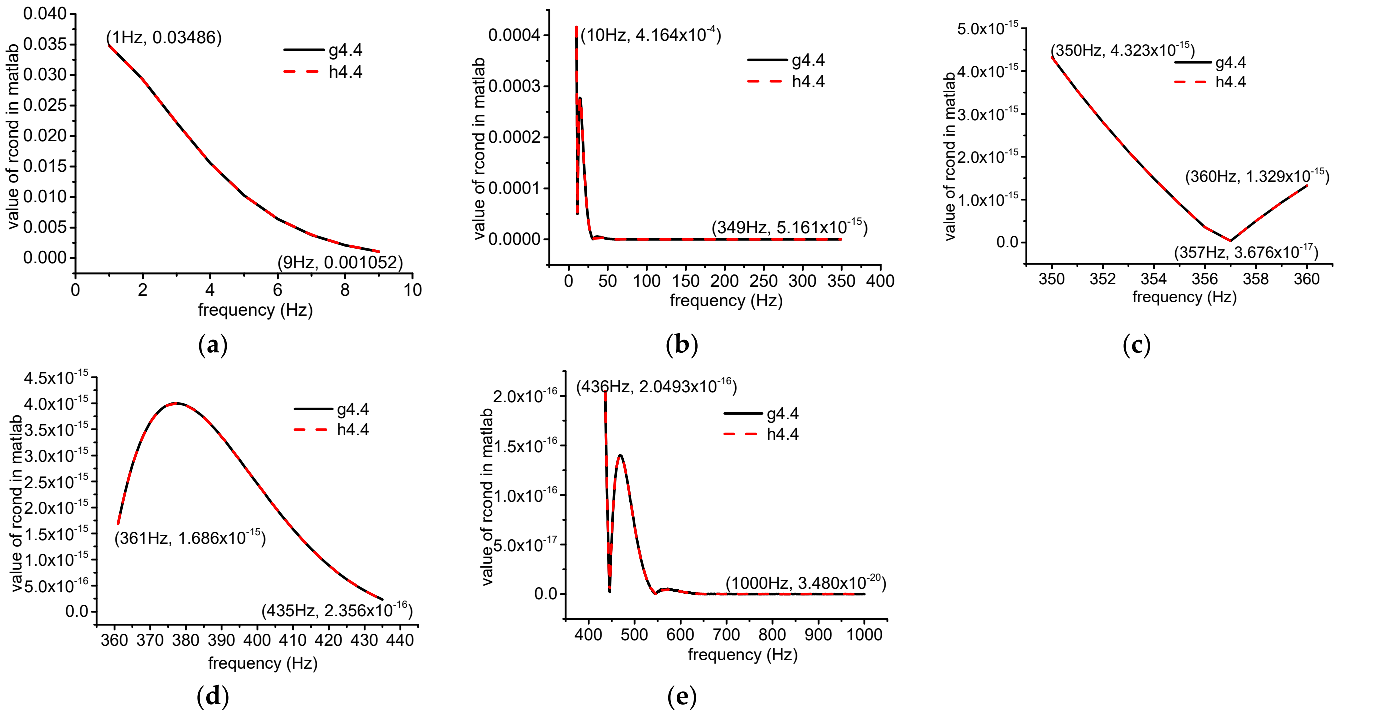

Figure 30. The reciprocal condition of the matrix M_{11}: (**a**) 1~9 Hz; (**b**) 10~349 Hz; (**c**) 350~360 Hz; (**d**) 361~435 Hz; (**e**) 436~1000 Hz.

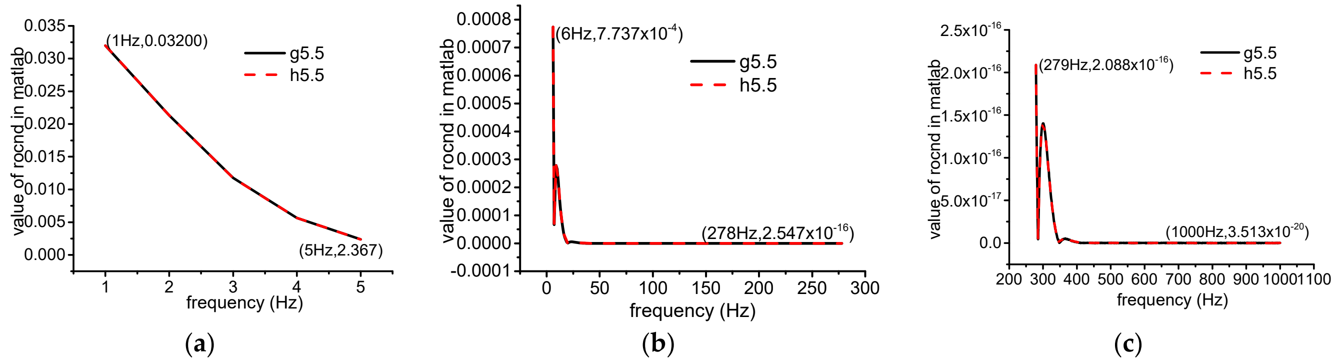

Figure 31. The reciprocal condition of the matrix M_{11}: (**a**) 1~9 Hz; (**b**) 6~278 Hz; (**c**) 279~1000 Hz.

According to Figures 28–31, the general trend is that the reciprocal condition of M_{11} decrease with the increase of frequency. It is indicated that M_{11} becomes more badly conditioned when the frequency increases. For g1.4, h1.4, g4.4 and h4.4, the alarm appears at 357 Hz and from 436 Hz to 1000 Hz. For g5.5 and h5.5, the alarms appear from 279 Hz to 1000 Hz. For g3.3 and h1.3, the alarms appear at 634 Hz and 635 Hz and from 774 Hz to 1000 Hz. Moreover, the reciprocal condition numbers of M_{11} are exactly equal at the same frequency for g4.4, h4.4, g1.4, h1.4. According to Equations (19) and (20) and Equation A1, the elements of the matrix M_{11} are only related to the parameters of the rotor-shaft and the rotating frequency. The parameters of shaft of the four rotors are same from Table 3. Consequently, similar rule can also be obtained from Figures 28–31. A possible solution of the singular M_{11} and the numerical stability is improving on calculation accuracy which is dependent on the development of Matlab software and computes. When using CRDAM, a proper alarm value of the reciprocal condition of M_{11} can be used to ignore the incorrect results due to the numerical stability.

3.4. Calculating Speed

Figure 32, which represents the time consumption of calculating unbalance response of each computational example by CRDAM, FEM, and Ricatti, is obtained. From Figure 32, the calculating speed of FEM is the slowest among the three methods. When calculating rotor g1.1, g2.2, g1.2, g1.3, h1.1, h2.2, h3.3, h1.2 and h1.3, the calculating speed of CRDAM is faster than that of Ricatti. When calculating rotor g3.3, g4.4, g5.5, g1.4, g1.5, h4.4, h5.5, h1.4 and h1.5, the calculating speed of CRDAM is slower than that of Ricatti. It means that when the rotor becomes complicated, the calculating speed of CRDAM is slower than of Ricatti. For example, calculating the unbalance response of rotor g5.5 and h5.5 by CRDAM needs 93.53 s and 231.8 s, respectively. However, it cost 34.91 s and 57.82 s using Ricatti. Moreover, the calculation time is very long for g5.5 and h5.5, which means complex rotors may take more calculation time than simple rotors when using CRDAM. The average time consumption of CRDAM, FEM and Ricatti is 44.64 s, 154.84 s and 30.45 s, respectively. Moreover, the time consumption of CRDAM increases with the complexity of the calculation instance according to Figure 32.

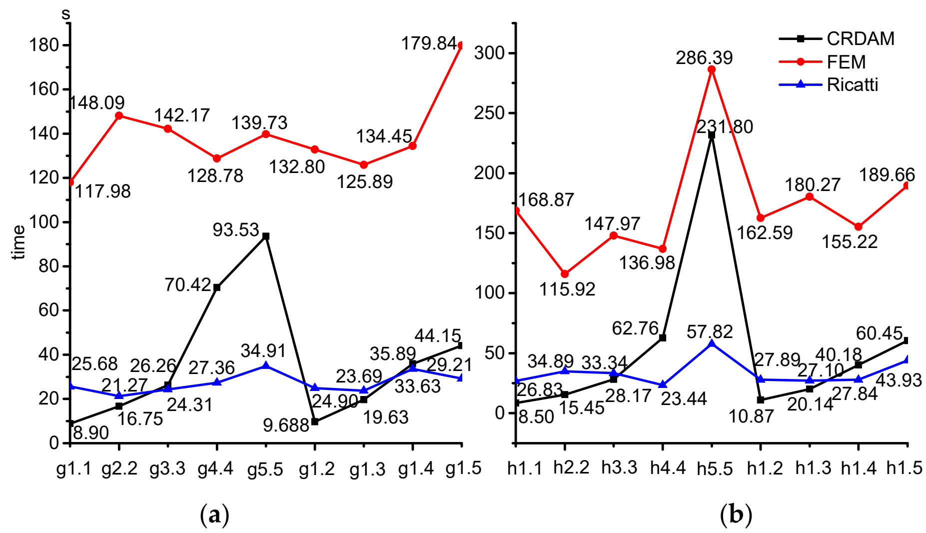

Figure 32. Time consumption of calculating the unbalance response from 0 Hz to 1000 Hz by CRDAM, FEM and Ricatti methods using the 18 computation examples: (**a**) for rotors with rolling bearings; (**b**) for rotors with oil journal bearings.

In addition, by dividing the shaft into more elements, more calculating time are needed for FEM and Ricatti, but the time consumption of CRDAM remains unchanged theoretically. Hence, the calculating speed of CRDAM can be the fastest.

4. Conclusions

For the multi-disc and multi-span rotor-bearing system, CRDAM, which can be used for further studies on identification of rotor unbalance and bearing coefficients, is proposed. Numerical experiments are conducted to validate the proposed method by comparing it with FEM and Ricatti. The results of this paper are concluded as follows:

(1) The functional relationship between the unbalance response and location on the shaft, rotor unbalance (amplitude and angle), each bearing's stiffness and damping coefficients and rotor's inherent parameters is obtained based on CRDAM.

(2) Numerical simulations indicate that the obtained unbalance response calculated by the three methods are almost equal when the frequency is away from the critical frequency, but they are different when the frequency is near the critical frequency. Moreover, CRDAM is closer to FEM than Ricatti. Although the critical frequencies calculated by them are almost equal to each other, the critical frequency calculated by CRDAM is closer to the critical frequency calculated by FEM than the critical

frequency obtained by Ricatti. The unbalance response obtained by CRDAM is also closer to the unbalance response obtained by FEM than the unbalance response by Ricatti, especially when the frequency is smaller than the low order frequency.

(3) Numerical simulations indicate that the calculating speed of CRDAM is the second fast among the three methods, but the speed of CRDAM becomes faster than Ricatti when the rotor is complicated. Simulations also show that the numerical stability of FEM and Ricatti is better than CRDAM. However, the numerical instability of CRDAM occurs when the frequency is high, often higher than the fifth order frequency.

In engineering practice, actual rotors work at the speed, which must be away from each critical frequency, to avoid sympathetic vibration. Hence, CRDAM is applicable to calculating unbalance response of multi-disc and multi-span rotor. High speed rotors are just across third critical frequency. Therefore, the proposed method can be applied to actual high speed rotors. However, complex rotor systems, such as the reducer gear transmission systems, which have multi shafts parallel in space, cannot be modelled by the proposed method. FEM and Ricatti should be applied for these complex rotors.

For further study, the loss factor could be considered for modelling the continuous rotor. Timoshenko model could be used in the model of the rotor. The forward problems of the continuous rotor dynamics for the multi-disc and multi-span rotors, is solved in this paper. Inverse problems of the continuous rotor dynamics could be conducted based the proposed CRDAM. For example, identification of rotor unbalance and bearing stiffness and damping of without test runs and external excitations, which has the advantages of easy implementation and low cost, should be studied in the future. It can be achieved by solving equations which are built using unbalance responses at some positions on rotor-shaft as known conditions based on the proposed functional relationship.

Author Contributions: Conceptualization, A.W.; methodology, A.W.; software, A.W., Y.B. and Y.X.; formal analysis, A.W.; investigation, Y.X., X.C. and J.Y.; writing—original draft preparation, A.W. and Y.B.; writing—review and editing, A.W. and Y.B.; supervision, G.M.; funding acquisition, G.M. All authors have read and agreed to the published version of the manuscript.

Funding: This research was funded by the Fundamental Research Funds for the Central Universities, grant number 8000150A084 and the Yue Qi Young Scholar Project, China University of Mining and Technology, Beijing, grant number 800015Z1145.

Institutional Review Board Statement: Not applicable.

Informed Consent Statement: Not applicable.

Data Availability Statement: The study did not report any data.

Conflicts of Interest: The authors declare no conflict of interest.

Appendix A

$$M_{11} = \begin{bmatrix} \sum\limits_{j=1}^{8} \frac{f_1(s_j)s_j^2}{f'(s_j)} e^{s_j} & \sum\limits_{j=1}^{8} \frac{f_2(s_j)s_j^2}{f'(s_j)} e^{s_j} & \sum\limits_{j=1}^{8} \frac{i \cdot KPs_j^3}{f'(s_j)} e^{s_j} & \sum\limits_{j=1}^{8} \frac{i \cdot KPs_j^2}{f'(s_j)} e^{s_j} \\ \sum\limits_{j=1}^{8} \frac{f_1(s_j)s_j^3}{f'(s_j)} e^{s_j} & \sum\limits_{j=1}^{8} \frac{f_2(s_j)s_j^3}{f'(s_j)} e^{s_j} & \sum\limits_{j=1}^{8} \frac{i \cdot KPs_j^4}{f'(s_j)} e^{s_j} & \sum\limits_{j=1}^{8} \frac{i \cdot KPs_j^3}{f'(s_j)} e^{s_j} \\ \sum\limits_{j=1}^{8} \frac{-i \cdot KP \cdot s_j^3}{f'(s_j)} e^{s_j} & \sum\limits_{j=1}^{8} \frac{-i \cdot KPs_j^2}{f'(s_j)} e^{s_j} & \sum\limits_{j=1}^{8} \frac{f_1(s_j)s_j^2}{f'(s_j)} e^{s_j} & \sum\limits_{j=1}^{8} \frac{f_2(s_j)s_j^2}{f'(s_j)} e^{s_j} \\ \sum\limits_{j=1}^{8} \frac{-i \cdot KP \cdot s_j^4}{f'(s_j)} e^{s_j} & \sum\limits_{j=1}^{8} \frac{-i \cdot KPs_j^3}{f'(s_j)} e^{s_j} & \sum\limits_{j=1}^{8} \frac{f_1(s_j)s_j^3}{f'(s_j)} e^{s_j} & \sum\limits_{j=1}^{8} \frac{f_2(s_j)s_j^3}{f'(s_j)} e^{s_j} \end{bmatrix} \tag{A1}$$

$$M_{12} = \begin{bmatrix} \sum\limits_{j=1}^{8} \frac{f_3(s_j)s_j^2}{f'(s_j)} e^{(1-q_i)s_j} \\ \sum\limits_{j=1}^{8} \frac{f_3(s_j)s_j^3}{f'(s_j)} e^{(1-q_i)s_j} \\ \sum\limits_{j=1}^{8} \frac{f_4(s_j)s_j^2}{f'(s_j)} e^{(1-q_i)s_j} \\ \sum\limits_{j=1}^{8} \frac{f_4(s_j)s_j^3}{f'(s_j)} e^{(1-q_i)s_j} \end{bmatrix} \tag{A2}$$

$$H_{11} = \begin{bmatrix} w^2 m_{1d} L G_u(q_{1d}, q_{1d}) & \cdots & w^2 m_{1d} L G_u(q_{md}, q_{1d}) \\ \vdots & \vdots & \vdots \\ w^2 m_{md} L G_u(q_{1d}, q_{md}) & \cdots & w^2 m_{md} L G_u(q_{md}, q_{md}) \end{bmatrix}_{m \times m} \tag{A3}$$

$$H_{12} = \begin{bmatrix} 0 & \cdots & 0 \\ \vdots & \vdots & \vdots \\ 0 & \cdots & 0 \end{bmatrix}_{m \times m} \tag{A4}$$

$$H_{13} = \begin{bmatrix} w^2 m_{1d} L G_u(q_{1b}, q_{1d}) & w^2 m_{1d} L G_u(q_{2b}, q_{1d}) & \cdots & w^2 m_{1d} L G_u(q_{nb}, q_{1d}) \\ \vdots & \vdots & \vdots & \vdots \\ w^2 m_{md} L G_u(q_{1b}, q_{md}) & w^2 m_{md} L G_u(q_{2b}, q_{md}) & \cdots & w^2 m_{md} L G_u(q_{nb}, q_{md}) \end{bmatrix}_{m \times n} \tag{A5}$$

$$H_{14} = \begin{bmatrix} 0 & \cdots & 0 \\ \vdots & \vdots & \vdots \\ 0 & \cdots & 0 \end{bmatrix}_{m \times n} \tag{A6}$$

$$H_{21} = \begin{bmatrix} 0 & \cdots & 0 \\ \vdots & \vdots & \vdots \\ 0 & \cdots & 0 \end{bmatrix}_{m \times m} \tag{A7}$$

$$H_{22} = \begin{bmatrix} w^2 m_{1d} L G_v(q_{1d}, q_{1d}) & \cdots & w^2 m_{1d} L G_v(q_{md}, q_{1d}) \\ \vdots & \vdots & \vdots \\ w^2 m_{md} L G_v(q_{1d}, q_{md}) & \cdots & w^2 m_{md} L G_v(q_{md}, q_{md}) \end{bmatrix}_{m \times m} \tag{A8}$$

$$H_{23} = \begin{bmatrix} 0 & \cdots & 0 \\ \vdots & \vdots & \vdots \\ 0 & \cdots & 0 \end{bmatrix}_{m \times n} \tag{A9}$$

$$H_{24} = \begin{bmatrix} w^2 m_{1d} L G_v(q_{1b}, q_{1d}) & w^2 m_{1d} L G_v(q_{2b}, q_{1d}) & \cdots & w^2 m_{1d} L G_v(q_{nb}, q_{1d}) \\ \vdots & \vdots & \vdots & \vdots \\ w^2 m_{md} L G_v(q_{1b}, q_{md}) & w^2 m_{md} L G_v(q_{2b}, q_{md}) & \cdots & w^2 m_{md} L G_v(q_{nb}, q_{md}) \end{bmatrix}_{m \times n} \tag{A10}$$

$$H_{31} = -L \begin{bmatrix} (k_{1 \cdot yy} + i \cdot wc_{1 \cdot yy}) G_u(q_{1d}, q_{1b}) & \cdots & (k_{1 \cdot yy} + i \cdot wc_{1 \cdot yy}) G_u(q_{md}, q_{1b}) \\ (k_{2 \cdot yy} + i \cdot wc_{2 \cdot yy}) G_u(q_{1d}, q_{2b}) & \cdots & (k_{2 \cdot yy} + i \cdot wc_{2 \cdot yy}) G_u(q_{md}, q_{2b}) \\ \vdots & \vdots & \vdots \\ (k_{n \cdot yy} + i \cdot wc_{n \cdot yy}) G_u(q_{1d}, q_{nb}) & \cdots & (k_{n \cdot yy} + i \cdot wc_{n \cdot yy}) G_u(q_{md}, q_{nb}) \end{bmatrix}_{n \times m} \tag{A11}$$

$$H_{32} = -L \begin{bmatrix} (k_{1 \cdot xy} + i \cdot wc_{1 \cdot xy}) G_v(q_{1d}, q_{1b}) & \cdots & (k_{1 \cdot xy} + i \cdot wc_{1 \cdot xy}) G_v(q_{md}, q_{1b}) \\ (k_{2 \cdot xy} + i \cdot wc_{2 \cdot xy}) G_v(q_{1d}, q_{2b}) & \cdots & (k_{2 \cdot xy} + i \cdot wc_{2 \cdot xy}) G_v(q_{md}, q_{2b}) \\ \vdots & \vdots & \vdots \\ (k_{n \cdot xy} + i \cdot wc_{n \cdot xy}) G_v(q_{1d}, q_{nb}) & \cdots & (k_{n \cdot xy} + i \cdot wc_{n \cdot xy}) G_v(q_{md}, q_{nb}) \end{bmatrix}_{n \times m} \tag{A12}$$

$$H_{33} = -L\begin{bmatrix} (k_{1\cdot yy} + i\cdot wc_{1\cdot yy})G_u(q_{1b}, q_{1b}) & (k_{1\cdot yy} + i\cdot wc_{1\cdot yy})G_u(q_{2b}, q_{1b}) & \cdots & (k_{1\cdot yy} + i\cdot wc_{1\cdot yy})G_u(q_{nb}, q_{1b}) \\ (k_{2\cdot yy} + i\cdot wc_{2\cdot yy})G_u(q_{1b}, q_{2b}) & (k_{2\cdot yy} + i\cdot wc_{2\cdot yy})G_u(q_{2b}, q_{2b}) & \cdots & (k_{2\cdot yy} + i\cdot wc_{2\cdot yy})G_u(q_{nb}, q_{2b}) \\ \vdots & \vdots & \vdots & \vdots \\ (k_{n\cdot yy} + i\cdot wc_{n\cdot yy})G_u(q_{1b}, q_{nb}) & (k_{n\cdot yy} + i\cdot wc_{n\cdot yy})G_u(q_{2b}, q_{nb}) & \cdots & (k_{n\cdot yy} + i\cdot wc_{n\cdot yy})G_u(q_{nb}, q_{nb}) \end{bmatrix}_{n\times n} \quad \text{(A13)}$$

$$H_{34} = -L\begin{bmatrix} (k_{1\cdot xy} + i\cdot wc_{1\cdot xy})G_v(q_{1b}, q_{1b}) & (k_{1\cdot xy} + i\cdot wc_{1\cdot xy})G_v(q_{2b}, q_{1b}) & \cdots & (k_{1\cdot xy} + i\cdot wc_{1\cdot xy})G_v(q_{nb}, q_{1b}) \\ (k_{2\cdot xy} + i\cdot wc_{2\cdot xy})G_v(q_{1b}, q_{2b}) & (k_{2\cdot xy} + i\cdot wc_{2\cdot xy})G_v(q_{2b}, q_{2b}) & \cdots & (k_{2\cdot xy} + i\cdot wc_{2\cdot xy})G_v(q_{nb}, q_{2b}) \\ \vdots & \vdots & \vdots & \vdots \\ (k_{n\cdot xy} + i\cdot wc_{n\cdot xy})G_v(q_{1b}, q_{nb}) & (k_{n\cdot xy} + i\cdot wc_{n\cdot xy})G_v(q_{2b}, q_{nb}) & \cdots & (k_{n\cdot xy} + i\cdot wc_{n\cdot xy})G_v(q_{nb}, q_{nb}) \end{bmatrix}_{n\times n} \quad \text{(A14)}$$

$$H_{41} = -L\begin{bmatrix} (k_{1\cdot yx} + i\cdot wc_{1\cdot yx})G_u(q_{1d}, q_{1b}) & \cdots & (k_{1\cdot yx} + i\cdot wc_{1\cdot yx})G_u(q_{md}, q_{1b}) \\ (k_{2\cdot yx} + i\cdot wc_{2\cdot yx})G_u(q_{1d}, q_{2b}) & \cdots & (k_{2\cdot yx} + i\cdot wc_{2\cdot yx})G_u(q_{md}, q_{2b}) \\ \vdots & \vdots & \vdots \\ (k_{n\cdot yx} + i\cdot wc_{n\cdot yx})G_u(q_{1d}, q_{nb}) & \cdots & (k_{n\cdot yx} + i\cdot wc_{n\cdot yx})G_u(q_{md}, q_{nb}) \end{bmatrix}_{n\times m} \quad \text{(A15)}$$

$$H_{42} = -L\begin{bmatrix} (k_{1\cdot xx} + i\cdot wc_{1\cdot xx})G_v(q_{1d}, q_{1b}) & \cdots & (k_{1\cdot xx} + i\cdot wc_{1\cdot xx})G_v(q_{md}, q_{1b}) \\ (k_{2\cdot xx} + i\cdot wc_{2\cdot xx})G_v(q_{1d}, q_{2b}) & \cdots & (k_{2\cdot xx} + i\cdot wc_{2\cdot xx})G_v(q_{md}, q_{2b}) \\ \vdots & \vdots & \vdots \\ (k_{n\cdot xx} + i\cdot wc_{n\cdot xx})G_v(q_{1d}, q_{nb}) & \cdots & (k_{n\cdot xx} + i\cdot wc_{n\cdot xx})G_v(q_{md}, q_{nb}) \end{bmatrix}_{n\times m} \quad \text{(A16)}$$

$$H_{43} = -L\begin{bmatrix} (k_{1\cdot yx} + i\cdot wc_{1\cdot yx})G_u(q_{1b}, q_{1b}) & (k_{1\cdot yx} + i\cdot wc_{1\cdot yx})G_u(q_{2b}, q_{1b}) & \cdots & (k_{1\cdot yx} + i\cdot wc_{1\cdot yx})G_u(q_{nb}, q_{1b}) \\ (k_{2\cdot yx} + i\cdot wc_{2\cdot yx})G_u(q_{1b}, q_{2b}) & (k_{2\cdot yx} + i\cdot wc_{2\cdot yx})G_u(q_{2b}, q_{2b}) & \cdots & (k_{2\cdot yx} + i\cdot wc_{2\cdot yx})G_u(q_{nb}, q_{2b}) \\ \vdots & \vdots & \vdots & \vdots \\ (k_{n\cdot yx} + i\cdot wc_{n\cdot yx})G_u(q_{1b}, q_{nb}) & (k_{n\cdot yx} + i\cdot wc_{n\cdot yx})G_u(q_{2b}, q_{nb}) & \cdots & (k_{n\cdot yx} + i\cdot wc_{n\cdot yx})G_u(q_{nb}, q_{nb}) \end{bmatrix}_{n\times n} \quad \text{(A17)}$$

$$H_{44} = -L\begin{bmatrix} (k_{1\cdot xx} + i\cdot wc_{1\cdot xx})G_v(q_{1b}, q_{1b}) & (k_{1\cdot xx} + i\cdot wc_{1\cdot xx})G_v(q_{2b}, q_{1b}) & \cdots & (k_{1\cdot xx} + i\cdot wc_{1\cdot xx})G_v(q_{nb}, q_{1b}) \\ (k_{2\cdot xx} + i\cdot wc_{2\cdot xx})G_v(q_{1b}, q_{2b}) & (k_{2\cdot xx} + i\cdot wc_{2\cdot xx})G_v(q_{2b}, q_{2b}) & \cdots & (k_{2\cdot xx} + i\cdot wc_{2\cdot xx})G_v(q_{2b}, q_{nb}) \\ \vdots & \vdots & \vdots & \vdots \\ (k_{n\cdot xx} + i\cdot wc_{n\cdot xx})G_v(q_{1b}, q_{nb}) & (k_{n\cdot xx} + i\cdot wc_{n\cdot xx})G_v(q_{2b}, q_{nb}) & \cdots & (k_{n\cdot xx} + i\cdot wc_{n\cdot xx})G_v(q_{nb}, q_{nb}) \end{bmatrix}_{n\times n} \quad \text{(A18)}$$

Appendix B

Table A1. Calculated critical frequencies of rotor g1.1 and h1.1.

			g1.1					h1.1		
Order	**CRDAM**	**FE**	**Ricatti**	**C/F(%)**	**R/F(%)**	**CRDAM**	**FEM**	**Ricatti**	**C/F(%)**	**R/F(%)**
1th	33	33	33	0.000	0.000	33	33	33	0.000	0.000
2th	209	209	209	0.000	0.000	212	212	212	0.000	0.000
3th	355	352	360	0.852	2.273	598	597	596	0.168	0.168

Table A2. Calculated critical frequencies of rotor g2.2 and h2.2.

			g2.2					h2.2		
Order	**CRDAM (Hz)**	**FEM (Hz)**	**Ricatti (Hz)**	**C/F (%)**	**R/F (%)**	**CRDAM (Hz)**	**FEM (Hz)**	**Ricatti (Hz)**	**C/F (%)**	**R/F (%)**
1th	16	16	16	0.000	0.000	16	16	16	0.000	0.000
2th	104	104	104	0.000	0.000	104	104	104	0.000	0.000
3th	294	294	294	0.000	0.000	295	295	295	0.000	0.000
4th	568	568	571	0.000	0.528	570	570	573	0.000	0.526
5th	774	773	777	0.129	0.517	799	798	799	0.125	0.125

Table A3. Calculated critical frequencies of rotor g3.3 and h3.3.

			g3.3					h3.3		
Order	**CRDAM**	**FE**	**Ricatti**	**C/F(%)**	**R/F(%)**	**CRDAM**	**FEM**	**Ricatti**	**C/F(%)**	**R/F(%)**
1th	14	14	14	0.000	0.000	92	92	92	0.000	0.000
2th	91	91	91	0.000	0.000	258	258	260	0.000	0.775
3th	256	256	258	0.000	0.781	433	433	436	0.000	0.693
4th	390	390	392	0.000	0.513	458	457	458	0.219	0.219
5th	431	431	434	0.000	0.696	562	562	567	0.000	0.890
6th	549	549	555	0.000	1.093	892	892	911	0.000	2.130
7th	928	916	962	1.310	5.022	947	934	982	1.392	5.139

Table A4. Calculated critical frequencies of rotor g4.4 and h4.4.

			g4.4					h4.4		
Order	**CRDAM**	**FE**	**Ricatti**	**C/F(%)**	**R/F(%)**	**CRDAM**	**FEM**	**Ricatti**	**C/F(%)**	**R/F(%)**
1th	143	143	144	0.000	0.699	265	265	267	0.000	0.755
2th	253	253	255	0.000	0.791	303	303	305	0.000	0.660
3th	259	259	260	0.000	0.386	451	451	458	0.000	1.552
4th	279	279	280	0.000	0.358	534	531	550	0.565	3.578
5th	447	447	454	0.000	1.566	/	/	/	/	/
6th	529	526	544	0.570	3.422	/	/	/	/	/
7th	739	738	759	0.136	2.846	/	/	/	/	/

Table A5. Calculated critical frequencies of rotor g5.5 and h5.5.

			g5.5					h5.5		
Order	**CRDAM**	**FE**	**Ricatti**	**C/F(%)**	**R/F(%)**	**CRDAM**	**FEM**	**Ricatti**	**C/F(%)**	**R/F(%)**
1th	171	171	172	0.000	0.585	122	122	123	0.000	0.820
2th	341	340	350	0.294	2.941	192	192	193	0.000	0.521
3th	484	483	497	0.207	2.899	199	199	200	0.000	0.503
4th	/	/	/	/	/	206	206	207	0.000	0.485
5th	/	/	/	/	/	243	241	242	0.830	0.415
6th	/	/	/	/	/	429	428	442	0.234	3.271

Table A6. Calculated critical frequencies of rotor g1.2 and h1.2.

			g1.2					h1.2		
Order	**CRDAM (Hz)**	**FEM (Hz)**	**Ricatti (Hz)**	**C/F (%)**	**R/F (%)**	**CRDAM (Hz)**	**FEM (Hz)**	**Ricatti (Hz)**	**C/F (%)**	**R/F (%)**
1th	22	22	22	0.000	0.000	22	22	22	0.000	0.000
2th	87	87	87	0.000	0.000	87	87	87	0.000	0.000
3th	198	198	199	0.000	0.505	198	198	199	0.000	0.505
4th	329	329	330	0.000	0.304	329	329	330	0.000	0.304
5th	517	517	520	0.000	0.580	518	517	521	0.193	0.774
6th	749	747	757	0.268	1.339	753	750	749	0.400	0.133
7th	952	948	963	0.422	1.582	965	960	977	0.521	1.771

Table A7. Calculated critical frequencies of rotor g1.3 and h1.3.

	g1.3					h1.3				
Order	**CRDAM**	**FE**	**Ricatti**	**C/F(%)**	**R/F(%)**	**CRDAM**	**FEM**	**Ricatti**	**C/F(%)**	**R/F(%)**
1th	10	10	10	0.000	0.000	10	10	10	0.000	0.000
2th	39	39	40	0.000	2.564	39	39	40	0.000	2.564
3th	86	86	86	0.000	0.000	86	86	86	0.000	0.000
4th	151	151	152	0.000	0.662	151	151	152	0.000	0.662
5th	225	225	226	0.000	0.444	225	225	226	0.000	0.444
6th	335	334	338	0.299	1.198	335	335	338	0.000	0.896
7th	425	424	429	0.236	1.179	426	425	431	0.235	1.412
8th	526	525	531	0.190	1.143	529	529	535	0.000	1.134
9th	686	683	700	0.439	2.489	691	688	705	0.436	2.471
10th	847	843	868	0.474	2.966	853	848	874	0.590	3.066

Table A8. Calculated critical frequencies of rotor g1.4 and h1.4.

	g1.4					h1.4				
Order	**CRDAM**	**FE**	**Ricatti**	**C/F(%)**	**R/F(%)**	**CRDAM**	**FEM**	**Ricatti**	**C/F(%)**	**R/F(%)**
1th	22	22	22	0.000	0.000	22	22	22	0.000	0.000
2th	49	49	49	0.000	0.000	49	49	49	0.000	0.000
3th	86	86	86	0.000	0.000	86	86	86	0.000	0.000
4th	125	125	126	0.000	0.800	125	125	126	0.000	0.800
5th	237	237	239	0.000	0.844	190	189	191	0.529	1.058
6th	298	298	301	0.000	1.007	238	238	240	0.000	0.840
7th	383	382	389	0.262	1.832	299	299	302	0.000	1.003
8th	470	469	480	0.213	2.345	384	384	391	0.000	1.823
9th	/	/	/	/	/	471	470	481	0.213	2.340

Table A9. Calculated critical frequencies of rotor g1.5 and h1.5.

	g1.5					h1.5				
Order	**CRDAM**	**FE**	**Ricatti**	**C/F(%)**	**R/F(%)**	**CRDAM**	**FEM**	**Ricatti**	**C/F(%)**	**R/F(%)**
1th	4	4	4	0.000	0.000	4	4	4	0.000	0.000
2th	14	14	14	0.000	0.000	14	14	14	0.000	0.000
3th	32	32	32	0.000	0.000	32	32	32	0.000	0.000
4th	81	81	82	0.000	1.235	55	55	55	0.000	0.000
5th	120	120	121	0.000	0.833	81	81	82	0.000	1.235
6th	153	153	154	0.000	0.654	120	120	121	0.000	0.833
7th	193	193	194	0.000	0.518	153	153	154	0.000	0.654
8th	245	245	249	0.000	1.633	193	193	195	0.000	1.036
9th	301	300	307	0.333	2.333	246	246	250	0.000	1.626
10th	/	/	/	/	/	301	301	308	0.000	2.326

Appendix C

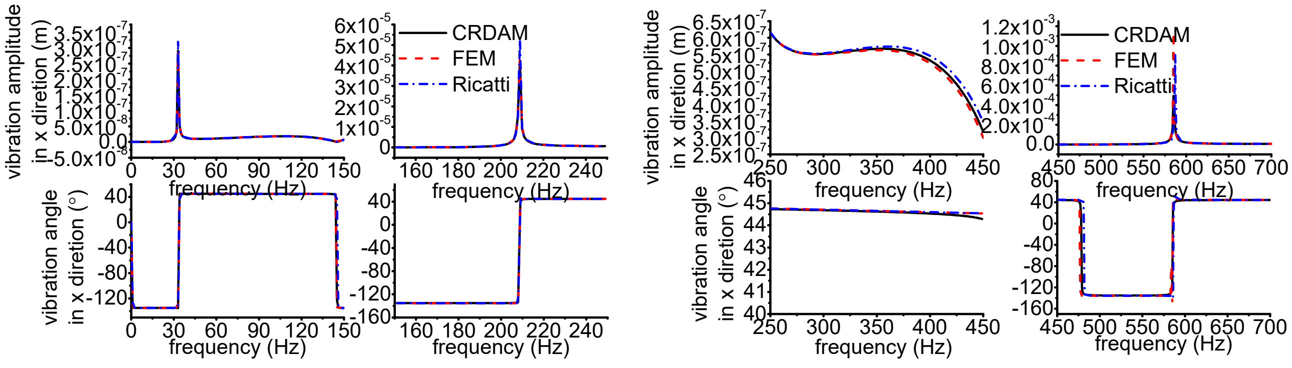

(**a**) (**b**) (**c**) (**d**)

Figure A1. *Cont.*

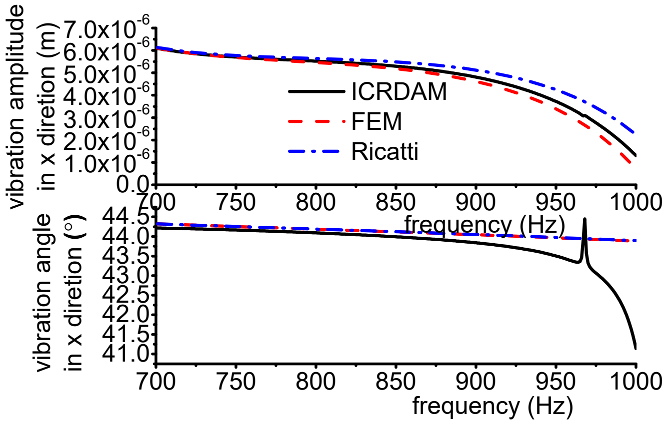

(**e**)

Figure A1. Unbalance response of point #2 in g1.1: (**a**) 0~150 Hz; (**b**) 150~250 Hz; (**c**) 250~450 Hz; (**d**) 450~700 Hz; (**e**) 700~1000 Hz.

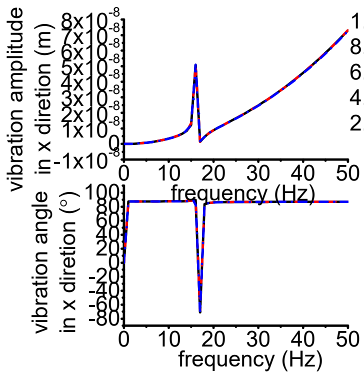

(**a**)

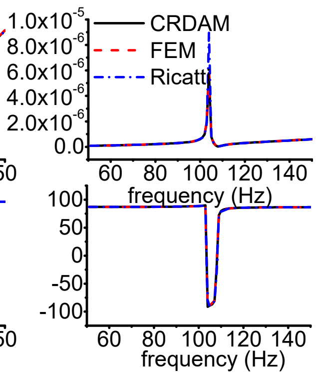

(**b**)

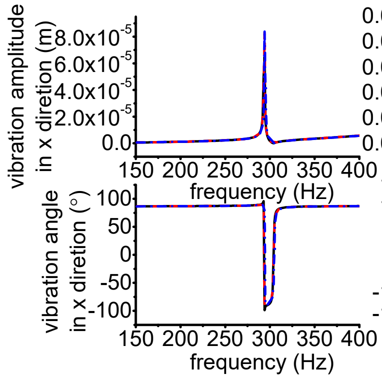

(**c**)

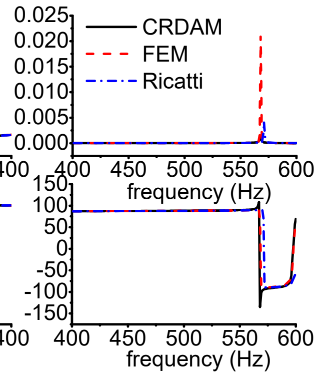

(**d**)

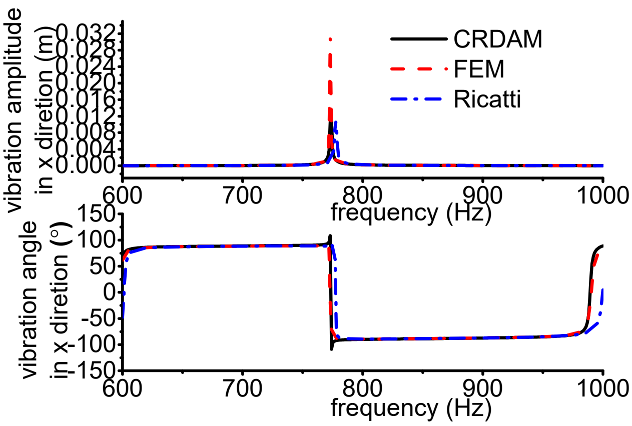

(**e**)

Figure A2. Unbalance response of point #2 in g2.2: (**a**) 0~50 Hz; (**b**) 50~150 Hz; (**c**) 150~400 Hz; (**d**) 400~600 Hz; (**e**) 600~1000 Hz.

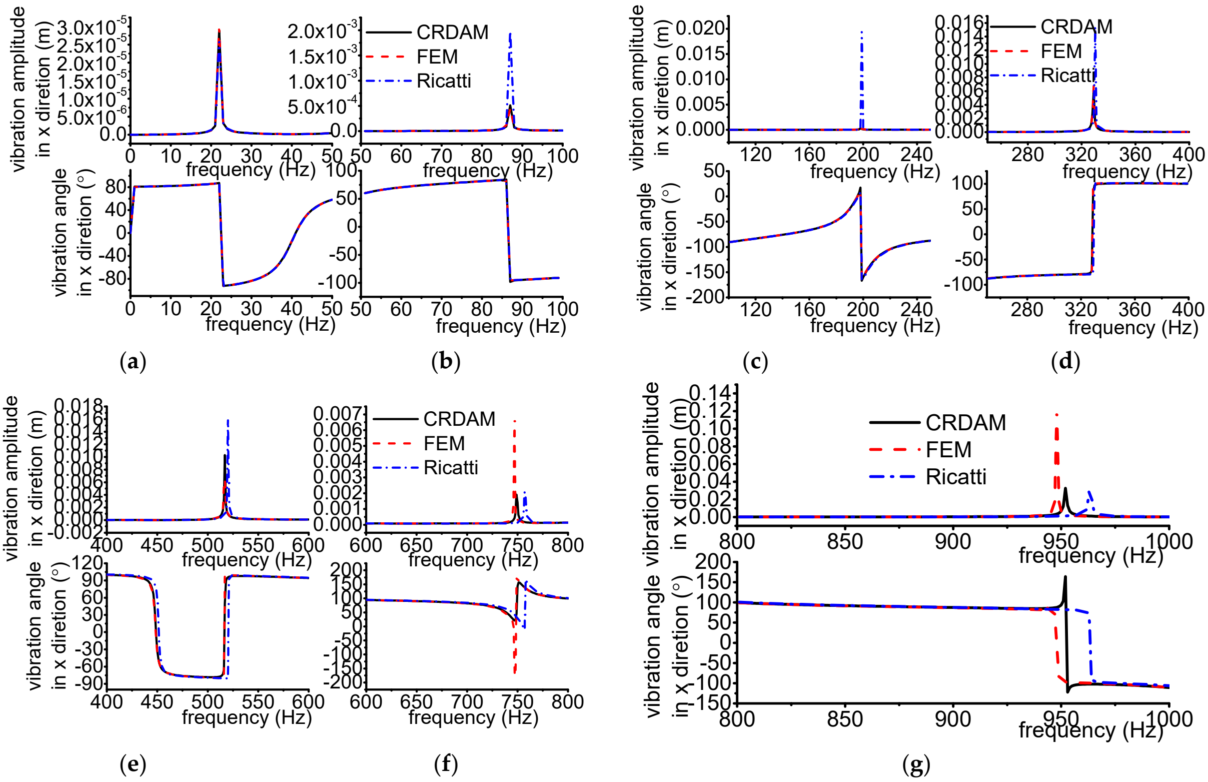

Figure A3. Unbalance response of point #2 in g1.2: (**a**) 0~50 Hz; (**b**) 50~100 Hz; (**c**) 100~250 Hz; (**d**) 250~400 Hz; (**e**) 400~600 Hz; (**f**) 600~800 Hz; (**g**) 800~1000 Hz.

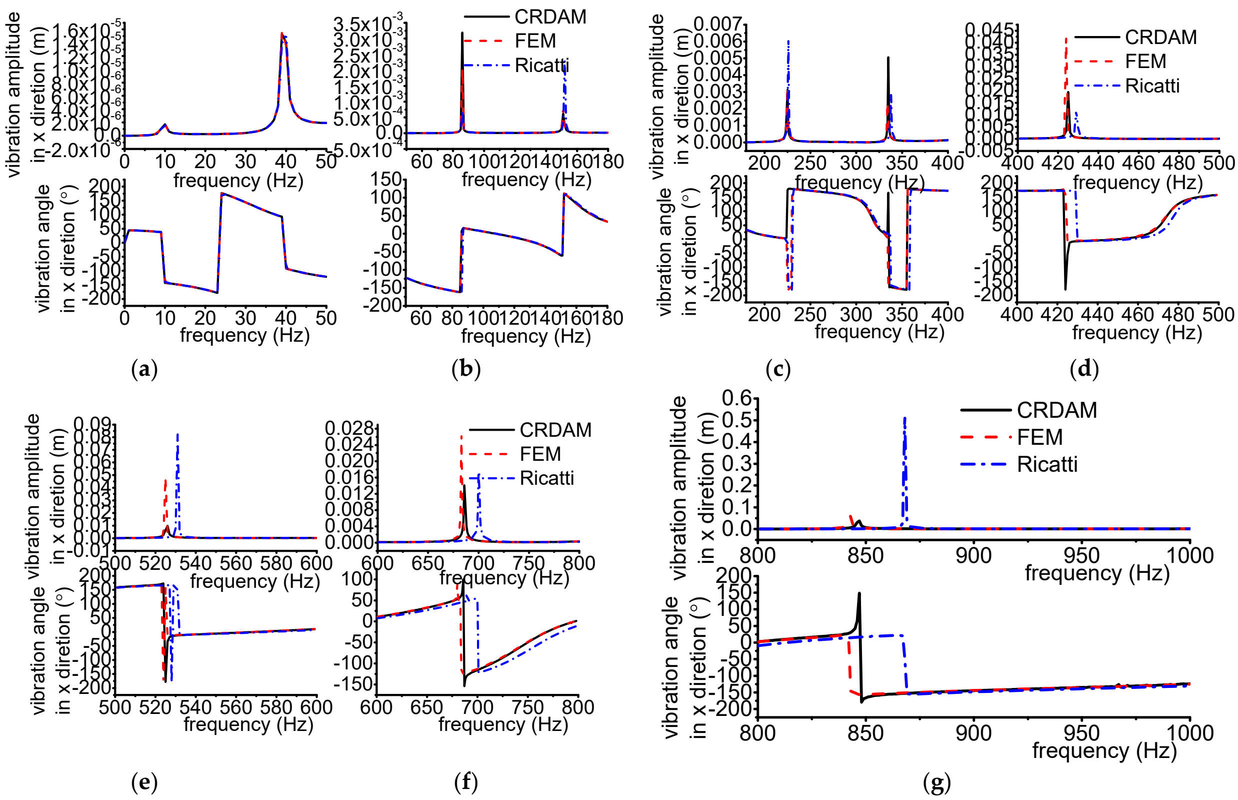

Figure A4. Unbalance response of point #2 in g1.3: (**a**) 0~50 Hz; (**b**) 50~180 Hz; (**c**) 180~400 Hz; (**d**) 400~500 Hz; (**e**) 500~600 Hz; (**f**) 600~800 Hz; (**g**) 800~1000 Hz.

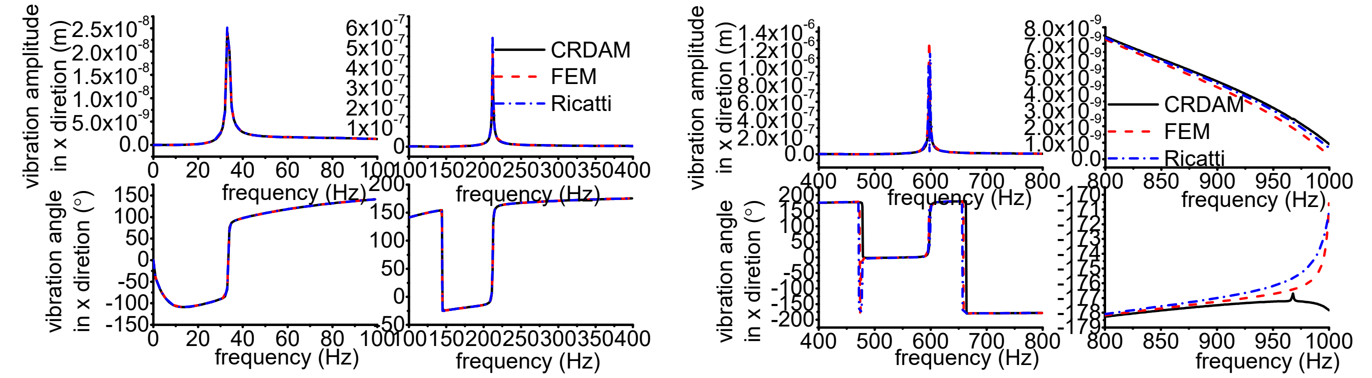

(**a**) (**b**) (**c**) (**d**)

Figure A5. Unbalance response of point #2 in h1.1: (**a**) 0~100 Hz; (**b**) 100~400 Hz; (**c**) 400~800 Hz; (**d**) 800~1000 Hz.

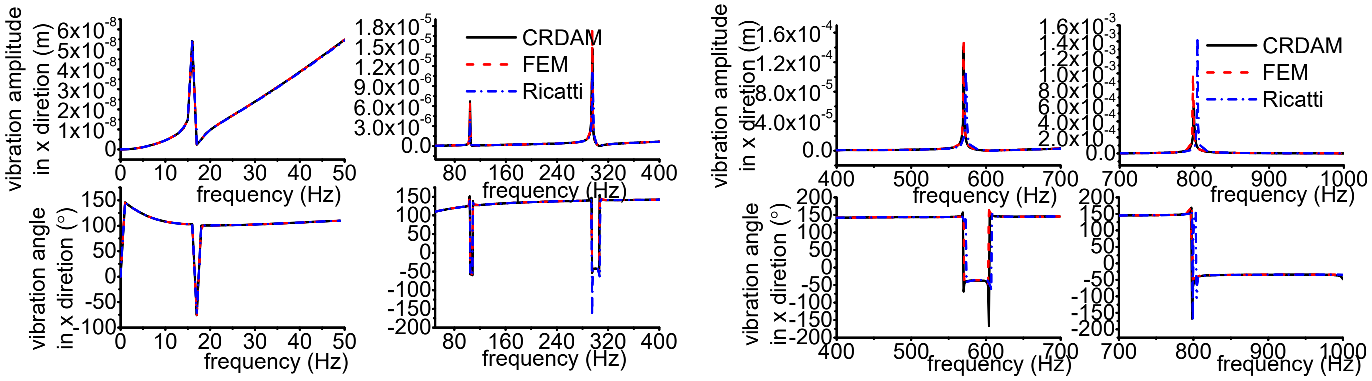

(**a**) (**b**) (**c**) (**d**)

Figure A6. Unbalance response of point #2 in h2.2: (**a**) 0~50 Hz; (**b**) 50~400 Hz; (**c**) 400~700 Hz; (**d**) 700~1000 Hz.

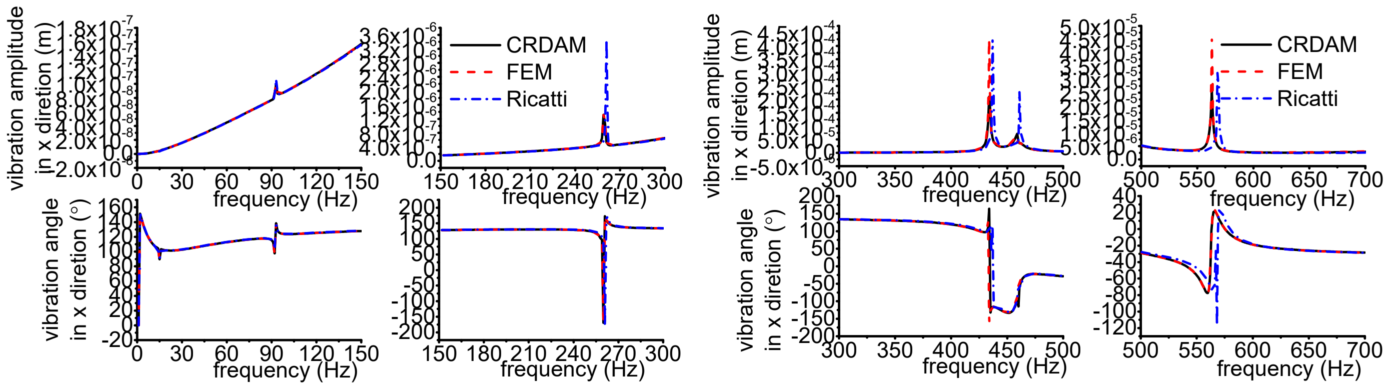

(**a**) (**b**) (**c**) (**d**)

Figure A7. *Cont.*

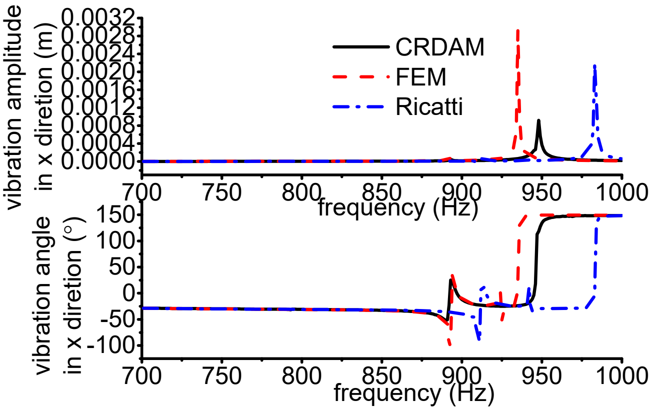

(**e**)

Figure A7. Unbalance response of point #2 in h3.3: (**a**) 0~150 Hz; (**b**) 150~300 Hz; (**c**) 300~500 Hz; (**d**) 500~700 Hz; (**e**) 700~1000 Hz.

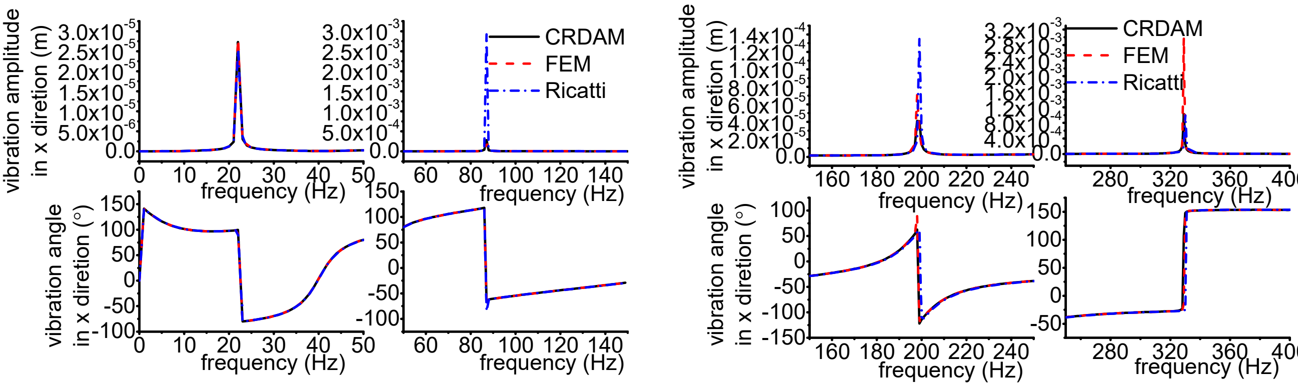

(**a**) (**b**) (**c**) (**d**)

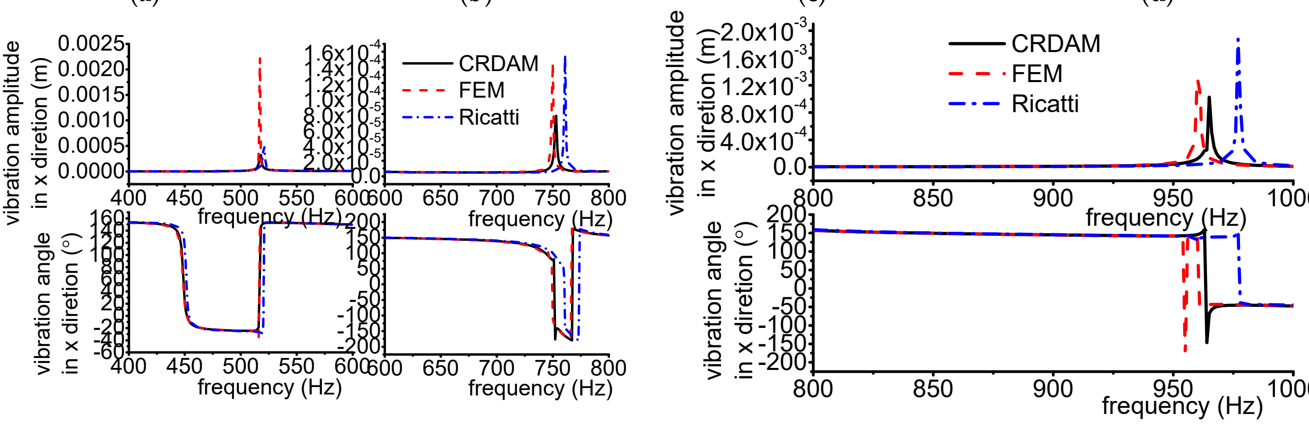

(**e**) (**f**) (**g**)

Figure A8. Unbalance response of point #2 in h1.2: (**a**) 0~50 Hz; (**b**) 50~150 Hz; (**c**) 150~250 Hz; (**d**) 250~400 Hz; (**e**) 400~600 Hz; (**f**) 600~800 Hz; (**g**) 800~1000 Hz.

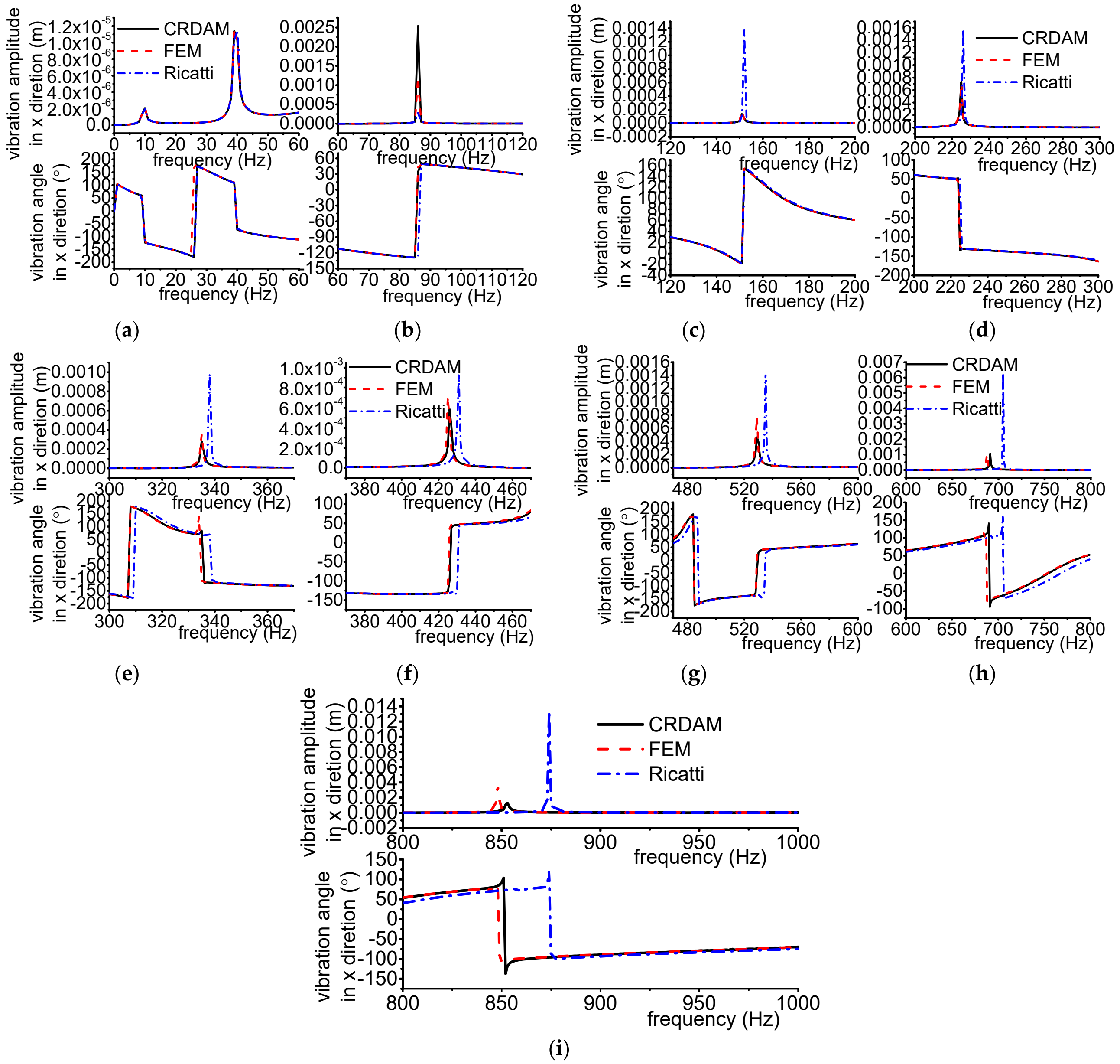

Figure A9. Unbalance response of point #2 in h1.3: (**a**) 0~60 Hz; (**b**) 60~120 Hz; (**c**) 120~200 Hz; (**d**) 200~300 Hz; (**e**) 300~370 Hz; (**f**) 370~470 Hz; (**g**) 370~600 Hz; (**h**) 600~800 Hz; (**i**) 800~1000 Hz.

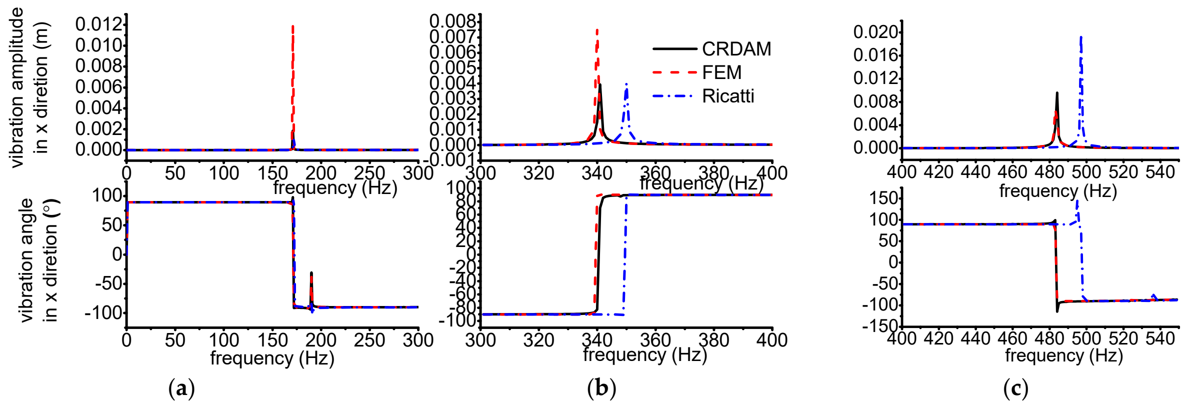

Figure A10. Unbalance response of point #2 in g5.5: (**a**) 0~300 Hz; (**b**) 300~400 Hz; (**c**) 400~550 Hz.

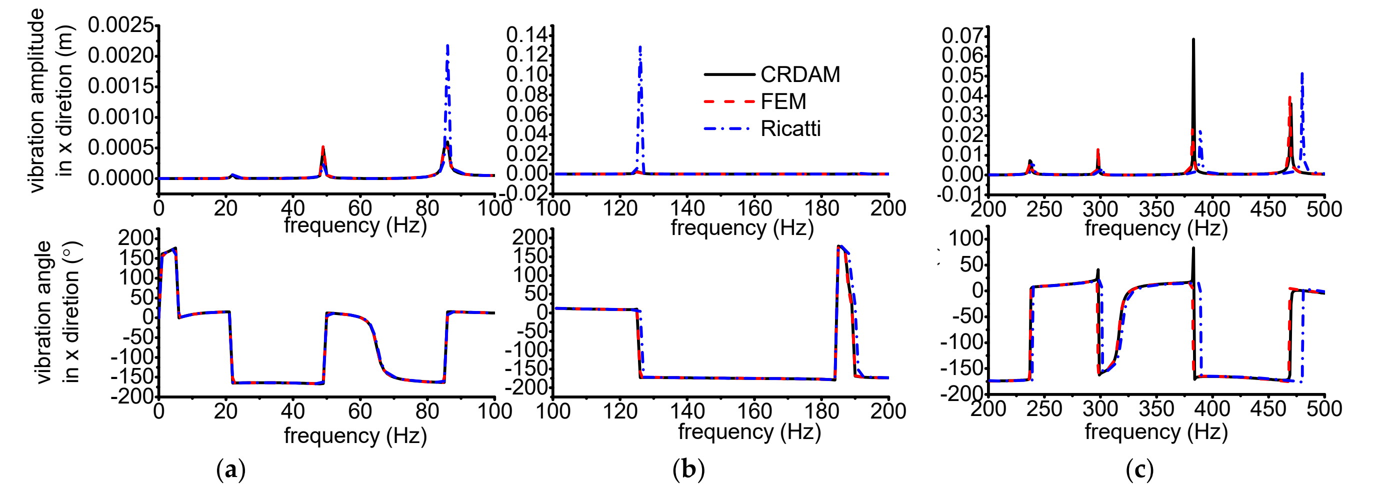

Figure A11. Unbalance response of point #2 in g1.4: (**a**) 0~100 Hz; (**b**) 100~200 Hz; (**c**) 200~500 Hz.

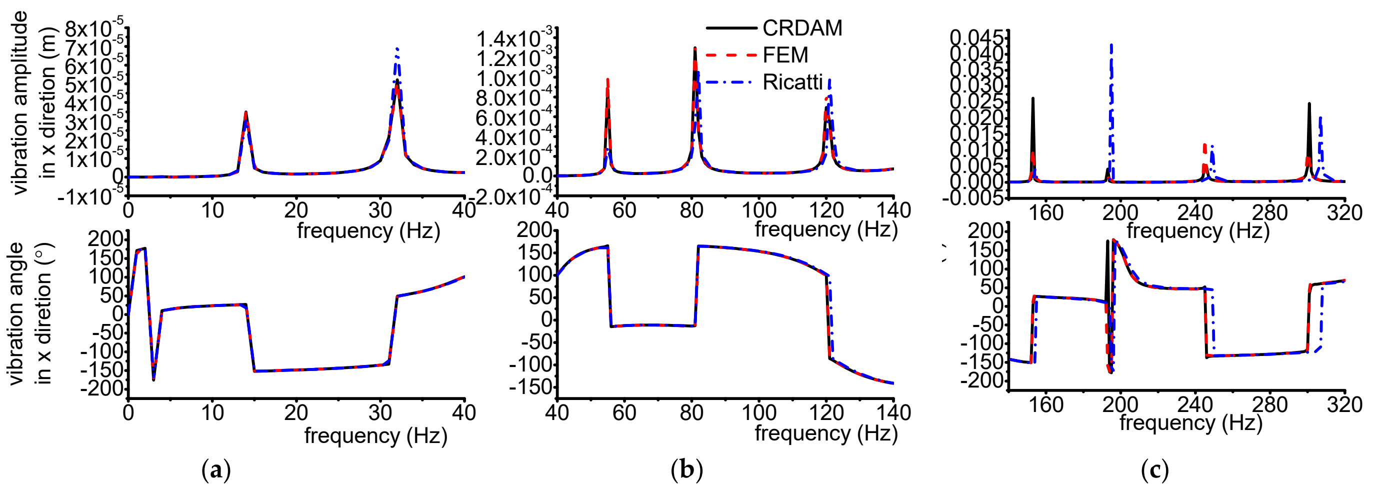

Figure A12. Unbalance response of point #2 in g1.5: (**a**) 0~40 Hz; (**b**) 40~140 Hz; (**c**) 140~320 Hz.

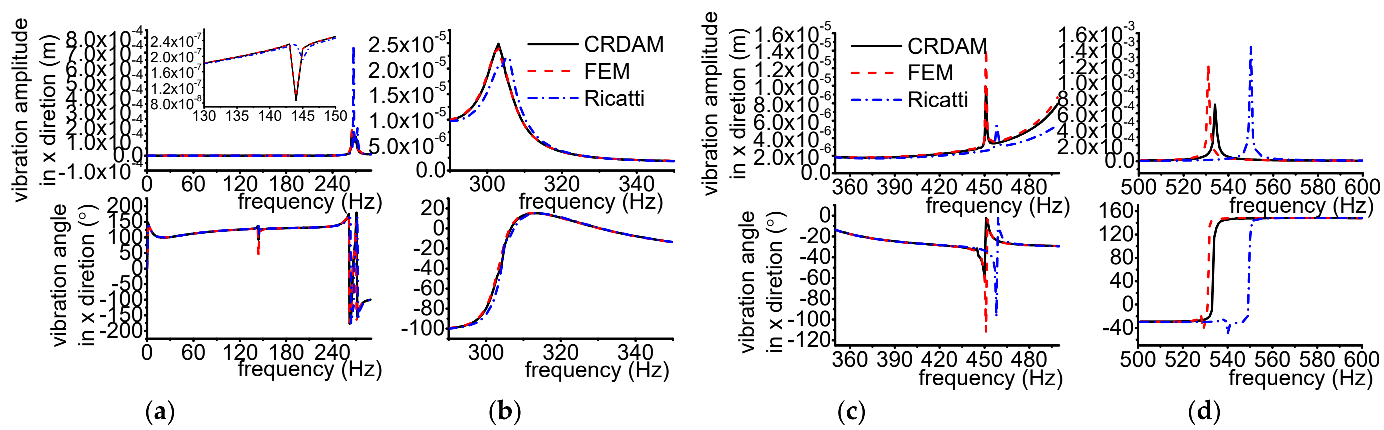

Figure A13. Unbalance response of point #2 in h4.4: (**a**) 0~290 Hz; (**b**) 290~350 Hz; (**c**) 350~500 Hz; (**d**) 500~600 Hz.

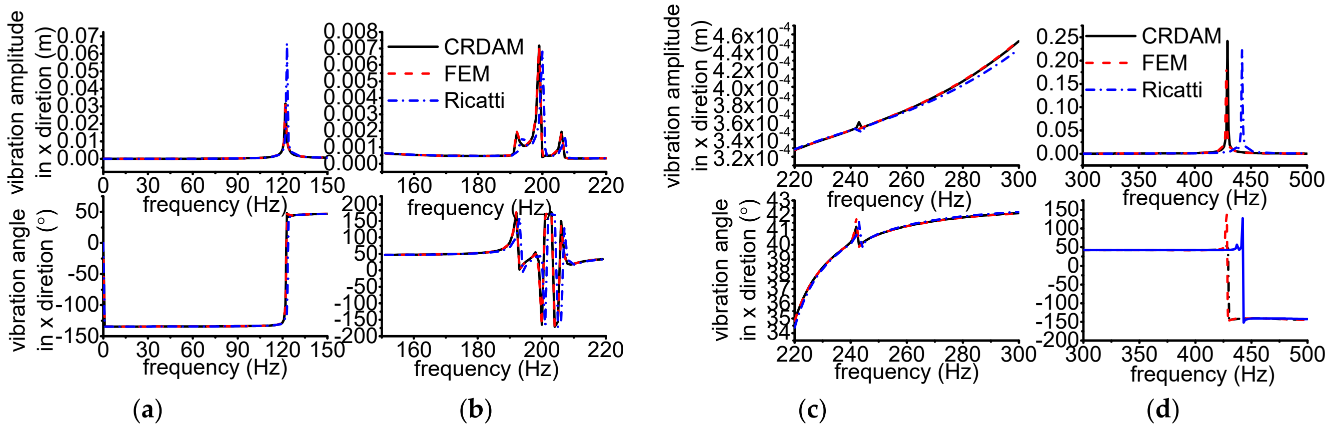

Figure A14. Unbalance response of point #2 in h5.5: (**a**) 0~150 Hz; (**b**) 150~220 Hz; (**c**) 220~300 Hz; (**d**) 300~500 Hz.

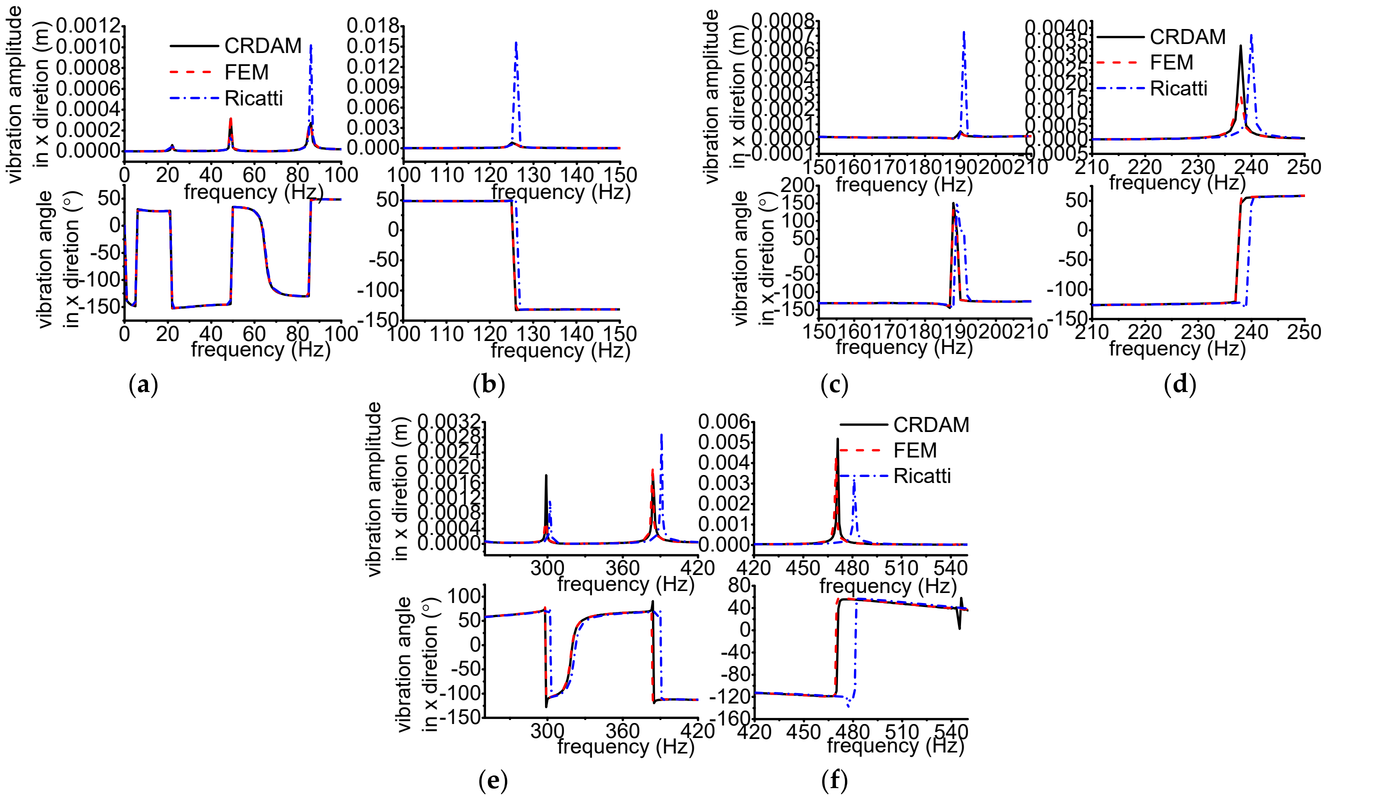

Figure A15. Unbalance response of point #2 in h1.4: (**a**) 0~100 Hz; (**b**) 100~150 Hz; (**c**) 150~210 Hz; (**d**) 210~250 Hz; (**e**) 250~420 Hz; (**f**) 420~540 Hz.

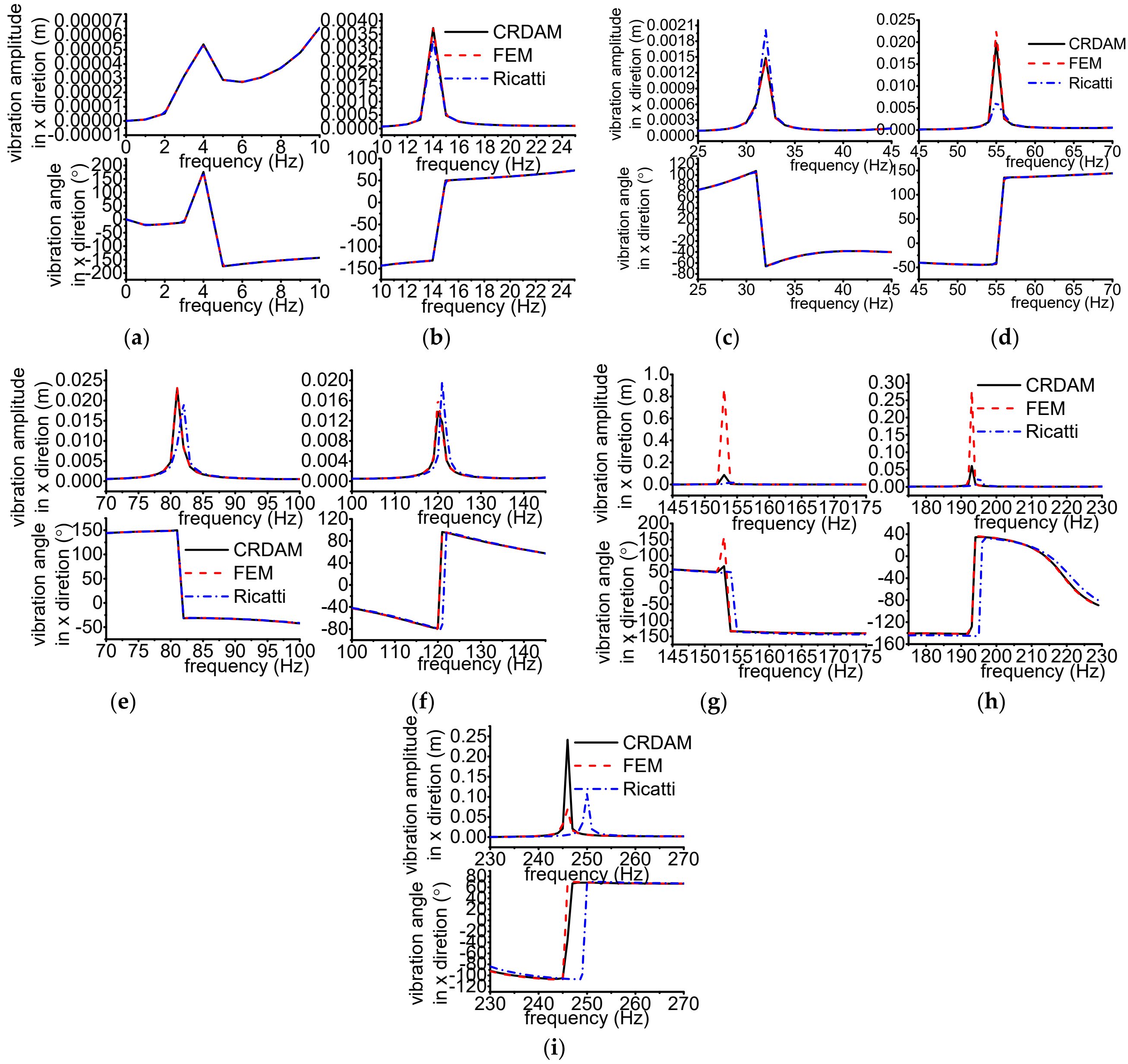

Figure A16. Unbalance response of point #2 in h1.5: (**a**) 0~10 Hz; (**b**) 10~25 Hz; (**c**) 25~45 Hz; (**d**) 45~70 Hz; (**e**) 70~100 Hz; (**f**) 100~145 Hz; (**g**) 145~175 Hz; (**h**) 175~230 Hz; (**i**) 230~270 Hz.

References

1. Horner, G.C.; Pilkey, W.D. The riccati transfer matrix method. *J. Mech. Des. Trans. ASME* **1978**, *100*, 297–302. [CrossRef]
2. Guptak, K.; Guptak, D. Unbalance response of a dual rotor system: Theory and experiment. *J. Vib. Acous. Trans. ASME* **1993**, *115*, 427–435. [CrossRef]
3. Behzad, M.; Mehri, B. Accuracy of the riccati transfer matrix method in rotor dynamic analysis. In *Turbo Expo: Power for Land, Sea, and Air*; American Society of Mechanical Engineers: New York, NY, USA, 1998; Volume 78668.
4. Lee, J.W.; Lee, J.Y. An exact transfer matrix expression for bending vibration analysis of a rotating tapered beam. *Appl. Math. Model.* **2018**, *53*, 167–188. [CrossRef]
5. Chen, G.; Zeng, X.; Liu, X.; Rui, X. Transfer matrix method for the free and forced vibration analyses of multi-step timoshenko beams coupled with rigid bodies on springs. *Appl. Math. Model.* **2020**, *87*, 152–170. [CrossRef]
6. Cao, H.; Niu, L.; Xi, S.; Chen, X. Mechanical model development of rolling bearing-rotor systems: A review. *Mech. Syst. Signal Process.* **2018**, *102*, 37–58. [CrossRef]
7. Nelson, H.D.; McVaugh, J.M. The dynamics of rotor-bearing systems using finite elements. *J. Eng. Ind. -Trans. ASME* **1976**, *5*, 593–600. [CrossRef]

8. Fan, H.; Zhang, X. Analysis of Imbalance Response of the Rotor Test Bed. In Proceedings of the 2008 IEEE/ASME International Conference on Advanced Intelligent Mechatronics, Xi'an, China, 2–5 July 2008; Volume 7, pp. 780–785.
9. Sekhar, A.S.; Prabhu, B.S. Unbalance response of rotors considering the distributed bearing stiffness and damping. In *Turbo Expo: Power for Land, Sea, and Air*; American Society of Mechanical Engineers: New York, NY, USA, 1994; Volume 78873.
10. Tan, X.; He, J.; Xi, C.; Deng, X.; Xi, X.; Chen, W.; He, H. Dynamic modeling for rotor-bearing system with electromechanically coupled boundary conditions. *Appl. Math. Model.* **2021**, *91*, 280–296. [CrossRef]
11. Zhou, W.; Qiu, N.; Wang, L.; Gao, B.; Liu, D. Dynamic analysis of a planar multi-stage centrifugal pump rotor system based on a novel coupled model. *J. Sound Vib.* **2018**, *434*, 237–260. [CrossRef]
12. Han, B.; Ding, Q. Forced responses analysis of a rotor system with squeeze film damper during flight maneuvers using finite element method. *Mech. Mach. Theory* **2018**, *122*, 233–251. [CrossRef]
13. Briend, Y.; Dakel, M.; Chatelet, E.; Andrianoely, M.-A.; Dufour, R.; Baudin, S. Effect of multi-frequency parametric excitations on the dynamics of on-board rotor-bearing systems. *Mech. Mach. Theory* **2020**, *145*, 103660. [CrossRef]
14. Fang, T.; Xue, P. *Theory of Vibration and Its Application*; Northwestern Polytechnical University Press: Xi'an, China, 1998.
15. Zhang, W. *The Theory of Rotor Dynamics*; Science Press: Beijing, China, 1990.
16. Yu, L. *Bearing-Rotor System Dynamics*; Xi'an Jiao Tong University Press: Xi'an, China, 2001.
17. Zhong, Y.; He, Y.; Wang, Z.; Li, F. *Rotor Dynamics*; Tsinghua University Press: Beijing, China, 1987.
18. Wen, B.; Gu, J.; Xia, S.; Wang, Z. *Advanced Rotor Dynamics: Theory, Technology and Application*; Machinery Industry Press: Beijing, China, 1999.
19. Timoshenko, S. *Vibration Problems in Engineering*; People's University Press: Beijing, China, 1978.
20. Vaz, J.C.; de Lima Junior, J.J. Vibration analysis of Euler-Bernoulli beams in multiple steps and different shapes of cross section. *J. Vib. Control* **2016**, *22*, 193–204. [CrossRef]
21. Heydari, H.; Khorram, A. Effects of location and aspect ratio of a flexible disk on natural frequencies and critical speeds of a rotating shaft-disk system. *Int. J. Mech. Sci.* **2019**, *152*, 596–612. [CrossRef]
22. Varanis, M.; Mereles, A.; Silva, A.; Balthazar, J.M.; Tusset, A.M. Rubbing Effect Analysis in a Continuous Rotor Model. In *Proceedings of the New Advances in Mechanism and Machine Science*; Springer Science and Business Media LLC: Cham, Switzerland, 2018; pp. 387–399.
23. Zhou, S.; Shi, J. The Analytical Imbalance Response of Jeffcott Rotor During Acceleration. *J. Manuf. Sci. Eng.* **2000**, *123*, 299–302. [CrossRef]
24. Lee, H.P. Divergence of a rotating shaft with an intermediate support and conservative axial loads. *Comput. Methods Appl. Mech. Eng.* **1993**, *110*, 317–324. [CrossRef]
25. Lee, H.P. Dynamic stability of spinning pre-twisted beams. *Int. J. Solids Struct.* **1994**, *31*, 2509–2517. [CrossRef]
26. Lee, H.P. Dynamic stability of spinning beams of unsymmetrical cross-section with distinct end conditions. *J. Sound Vib.* **1996**, *189*, 161–171. [CrossRef]
27. Chun, S.B.; Lee, C.W. Vibration analysis of shaft-bladed disk system by using substructure synthesis and assumed modes method. *J. Sound Vib.* **1996**, *189*, 587–608. [CrossRef]
28. Lee, C.W.; Chun, S.B. Vibration analysis of a rotor with multiple flexible disks using assumed modes method. *J. Vib. Acoust. -Trans. ASME* **1998**, *120*, 87–94. [CrossRef]
29. Hamidi, L.; Piaud, J.B.; Pastorel, H.; Mansour, W.M.; Massoud, M. Modal parameters for cracked rotors: Models and comparisons. *J. Sound Vib.* **1994**, *175*, 265–286. [CrossRef]
30. Wang, A.; Cheng, X.; Meng, G.; Xia, Y.; Wo, L.; Wang, Z. Dynamic analysis and numerical experiments for balancing of the continuous single-disc and single-span rotor-bearing system. *Mech. Syst. Signal Process.* **2017**, *86*, 151–176. [CrossRef]
31. Liao, H. The application of reduced space harmonic balance method for the nonlinear vibration problem in rotor dynamics. *Mech. Based Des. Struct. Mach.* **2019**, *47*, 154–174. [CrossRef]
32. Bouzidi, I.; Hadjoui, A.; Fellah, A. Dynamic analysis of functionally graded rotor-blade system using theclassical version of the finite element method. *Mech. Based Des. Struct. Mach.* **2020**, *49*, 1080–1108. [CrossRef]
33. Wang, A.; Yao, W.; He, K.; Meng, G.; Cheng, X.; Yang, J. Analytical modelling and numerical experiment for simultaneous identifi-cation of unbalance and rolling-bearing coefficients of the continuous single-disc and single-span rotor-bearing system with Rayleigh beam model. *Mech. Syst. Signal Process.* **2019**, *116*, 322–346. [CrossRef]
34. Mereles, A.; Cavalca, K.L. Mathematical modeling of continuous multi-stepped rotor-bearing systems. *Appl. Math. Model.* **2021**, *90*, 327–350. [CrossRef]
35. Mereles, A.; Cavalca, K.L. Modeling of multi-stepped rotor-bearing systems by the continuous segment method. *Appl. Math. Model.* **2021**, *96*, 402–430. [CrossRef]
36. Farghaly, S.H.; El-Sayed, T.A. Exact free vibration of multi-step timoshenko beam system with several attachments. *Mech. Syst. Signal Process.* **2016**, *72*, 525–546. [CrossRef]
37. Afshari, H.; Rahaghi, M.I. Whirling analysis of multi-span multi-stepped rotating shafts. *J. Braz. Soc. Mech. Sci. Eng.* **2018**, *40*, 424. [CrossRef]
38. Afshari, H.; Torabi, K.; Jazi, A.J. Exact closed form solution for whirling analysis of Timoshenko rotors with multiple concentrated masses. *Mech. Based Des. Struct. Mach.* **2020**, *50*, 969–992. [CrossRef]

39. Torabi, K.; Afshari, H.; Najafi, H. Whirling analysis of axial-loaded multi-step Timoshenko rotor carrying concentrated masses. *J. Solid Mech.* **2017**, *9*, 138–156.
40. Rao, D.K.; Swain, A.; Roy, T. Dynamic responses of bidirectional functionally graded rotor shaft. *Mech. Based Des. Struct. Mach.* **2020**, *50*, 302–330. [CrossRef]
41. De Felice, A.; Sorrentino, S. Damping and gyroscopic effects on the stability of parametrically excited continuous rotor systems. *Nonlinear Dyn.* **2021**, *103*, 3529–3555. [CrossRef]
42. Fung, R.F.; Hsu, S.M. Dynamic formulations and energy analysis of rotating flexible-shaft/multi-flexible-disk system with ed-dy-current brake. *J. Vib. Acoust. -Trans. ASME* **2000**, *122*, 365–375. [CrossRef]
43. Rao, S.S. *Vibration of Continuous Systems*; Wiley: New York, NY, USA, 2007.